Convection in binary fluids: Amplitude equations, codimension-2 bifurcation, and thermal fluctuations

Wolfgang Schöpf
Physikalisches Institut der Universität Bayreuth, W-8580 Bayreuth, Germany
and Centre for Water Research, University of Western Australia, Nedlands, Western Australia 6009, Australia

Walter Zimmermann
Institut für Festkörperforschung, Forschungszentrum Jülich, KFA, W-5170 Jülich, Germany
(Received 19 May 1992)

The near-threshold behavior for thermal convection in binary fluid mixtures heated from below is determined for realistic (rigid and impervious) boundary conditions at top and bottom. We calculate up to third order the coefficients of the amplitude equations for the stationary, the traveling-wave, and the standing-wave convection. In all three cases, the bifurcation changes with decreasing separation ratio Ψ from forward to backward with the respective tricritical points occurring for negative Ψ. For small values of the Lewis number L, these tricritical points, together with the codimension-2 point, lie near $\Psi=0$ and for $L=0$ they all degenerate to $\Psi=0$, which describes the limit of normal fluids. Near the codimension-2 point, where the thresholds for the stationary and the Hopf bifurcation coincide, a generalized amplitude equation has to be considered, whose nonrescaleable coefficients are determined from the already-known ones of the conventional amplitude equations. Some special properties of the traveling waves, such as the Benjamin-Feir instability and the sign change of the group velocity, can be deduced from the codimension-2 amplitude equation. Finally, the influence of thermal fluctuations on the convection onset is considered. We determine the strength of the additive noise term appearing in the amplitude equation for free and previous boundary conditions as well as for rigid and impervious boundary conditions for both the stationary bifurcation and the traveling waves. The space-time-correlation function for the order parameter below threshold is derived. Our calculated noise strength and correlation function agree rather well with the data of a recent experiment [W. Schöpf and I. Rehberg, Europhys. Lett. **17**, 321 (1992)].

PACS number(s): 47.20.−k, 47.27.Te, 03.40.Gc, 05.40.+j

I. INTRODUCTION

Understanding the common features of pattern formation in spatially extended, dissipative nonequilibrium systems subjected to an external stress R is a major challenge. In such systems, patterns can arise when R exceeds a critical value R_c (for numerous examples and references see, e.g., Ref. [1]). One class of laboratory systems is fluid-dynamical ones such as Rayleigh-Bénard convection [2,3] in isotropic (e.g., water) [4] or in intrinsically anisotropic fluids (e.g., nematic liquid crystals) [5]. Besides these thermally driven systems, Taylor-Couette flow [3,6] and electrohydrodynamic convection in nematic liquid crystals [7] play an important role. In contrast to natural ones, these physical systems have the advantage of great experimental flexibility. They are often accessible to highly accurate measurements, which makes a comparison with results obtained from the known fundamental equations possible.

An interesting system that has attracted much attention during recent years is thermal convection in a horizontal layer of a binary fluid [8,9]. This is a mixture of two (miscible) fluids such as, e.g., water-alcohol or ^{3}He-^{4}He. Owing to the two-component nature one has the Soret effect, and this leads to an additional control parameter besides the Rayleigh number R, namely, the separation ratio Ψ, which is a measure for the stabilizing ($\Psi<0$) or destabilizing ($\Psi>0$) effect of concentration gradients [8,9]. Depending on Ψ, above a critical temperature difference, convection may set in as a stationary roll pattern or via a Hopf bifurcation leading to time-periodic states [8,9], which in the simplest case can manifest themselves as traveling waves (TW's) or standing waves (SW's) [10]. The interest in observing a direct transition from a thermally conductive to an oscillating convective state together with the possibility of a codimension-2 bifurcation, where the thresholds for the stationary and the Hopf bifurcation coincide, has led to a large number of experiments during recent years [9,11–18]. This development was accompanied by considerable progress in the theoretical understanding [10,19–30]. Analysis on the phenomenological level [30,31] or on the level of symmetry considerations [10,32] often provided important insights. Nevertheless it became important to calculate also various properties of the transition to convection quantitatively from the fundamental equations. These *ab initio* calculations can be divided into mode truncations [21,22,33], full numerical simulations of the Navier-Stokes equations [26], and symmetry-aided systematic perturbation expansions around some bifurcation points of interest [31,34–41]. These approaches are all valuable, with restrictions and complementary advantages.

The transitions from a conductive to a convective state share many properties with thermodynamic equilibrium

phase transitions, so they are often referred to as nonequilibrium phase transitions. Linearizing the full hydrodynamic equations around the basic (the pure thermal conducting) state yields, for a periodic perturbation $\propto e^{\sigma t+ikx}$, a characteristic polynomial for the growth rate σ (we consider only the problem of quasi-one-dimensional pattern formation, where the wave vector $\mathbf{k}$ describing the structure points into a fixed direction, e.g., the x direction). The transition takes place where the real part of one or two roots passes through zero. In the case of a forward bifurcation, the linear modes with positive $\mathrm{Re}(\sigma)$ saturate above the transition, whereas all other modes are damped out. The spatiotemporal behavior of these growing linear modes characterizes the convecting pattern near threshold, where in its neighborhood they obey the so-called amplitude equations [31,34]. These are obtained from a perturbation expansion of the underlying fluid equations for small amplitudes. To lowest order they have a form analogous to the Ginzburg-Landau equation for equilibrium phase transitions; therefore they are also called generalized or complex Ginzburg-Landau equations. The rather general case of a pair of complex-conjugate eigenvalues σ with $\mathrm{Re}(\sigma)=0$ (Hopf bifurcation) leads to two coupled equations for the complex amplitudes of the linear modes [30,42]:

$$\tau_0(\partial_t-v_g\partial_x)A=\epsilon(1+ic_0)A+\xi_0^2(1+ic_1)\partial_x^2 A -(\alpha+ic_2)|A|^2A-(\gamma+ic_3)|B|^2A\ , \tag{1.1a}$$

$$\tau_0(\partial_t+v_g\partial_x)B=\epsilon(1+ic_0)B+\xi_0^2(1+ic_1)\partial_x^2 B -(\alpha+ic_2)|B|^2B-(\gamma+ic_3)|A|^2B\ . \tag{1.1b}$$

Here ε is the scaled control parameter describing the relative distance from the bifurcation point: $\varepsilon=(R-R_c)/R_c$. With $A(x,t)$ being the amplitude of the left traveling wave $(e^{i(\omega t+kx)})$ and $B(x,t)$ the amplitude of the right traveling wave $(e^{i(\omega t-kx)})$, these equations describe modulations of the waves on a slow time and space scale for a Hopf bifurcation. The special cases of pure traveling waves ($A=0$ or $B=0$) and standing waves ($A=\pm B$) can be recovered. The nonlinear Schrödinger equation is included as a limiting case ($A=0$ or $B=0$; $c_1,c_2\to\infty$). In its general form, Eqs. (1.1a) and (1.1b) cannot be derived from a potential. For $v_g=c_0=c_1=c_2=c_3=\gamma=0$ they combine into a single equation for the stationary bifurcation, where they have a potential. This form is also well known as the Ginzburg-Landau equation for a neutral superfluid. The amplitude equations can in principle be derived by symmetry arguments [31,42], thus being valid for a large class of pattern-forming systems. Of course, the actual values of the parameters depend on the special system.

In this paper we focus on the transition from the conductive to the convective state for both the stationary and the Hopf bifurcation of a binary fluid mixture heated from below. We consider a system of infinite horizontal extent with realistic (rigid and impermeable) boundary conditions on top and bottom. We analyze the linear stability of the conductive state (see also Refs. [19,24,25]) from which the linear coefficients of Eqs. (1.1a) and (1.1b) can be derived and which are the basis for further calculations. There exists a large amount of literature on the solution properties of Eqs. (1.1a) and (1.1b) [30,39,42–47]. However, the nonrescaleable nonlinear parameters, which are the sign of α, the ratio c_2/α, γ, and c_3, were not known for realistic boundary conditions. Thus we present here a full set of coefficients of Eqs. (1.1a) and (1.1b) for appropriately chosen fluid parameters with emphasis on the nonlinear coefficients (part of the results was given in Ref. [28]; the linear coefficients have already been discussed for the Hopf bifurcation in great detail in Ref. [25]).

Near the codimension-2 point (CTP) the conductive state becomes unstable against both a stationary and an oscillatory mode, i.e., the real parts of two eigenvalues pass through zero nearly simultaneously. This violates the assumptions made for deriving amplitude equations such as Eqs. (1.1a) and (1.1b). Instead a new equation, now second order in time, has to be used near the CTP (see, e.g., Refs. [37,38,40,41]; in Ref. [41] the terms with $\tilde g_1$, $\tilde g_3$, $\tilde f_4$, and $\tilde f_5$ have been neglected, in Ref. [40] the equation was discussed without spatial derivatives and with $P_k=0$, and in Ref. [38] additionally f_3 was set equal to zero):

$$\partial_T^2\tilde A-\eta[r+(\partial_X-iP_k)^2]\partial_T\tilde A+\eta(f_2+f_3)|\tilde A|^2\partial_T\tilde A+\eta f_3\tilde A^2\partial_T\tilde A^* -[(r+s)(1-i\eta\tilde g_1\partial_X)+a\partial_X^2-i\eta\tilde g_3\partial_X^3-f_1|\tilde A|^2]\tilde A-i\eta\tilde f_4|\tilde A|^2\partial_X\tilde A-i\eta\tilde f_5\tilde A^2\partial_X\tilde A^*=0\ . \tag{1.2}$$

This leads to a richer dynamical behavior, which is expected also from general mathematical considerations [48]. In this formulation the CTP is at $s=0$. P_k describes the wave-number difference between the unstable stationary and oscillatory modes and fixes the magnitude of the formal expansion parameter η (see Sec. IV). X and T are appropriately scaled space and time coordinates (see Sec. IV) and the coefficients depend on the physical system. $\tilde A(X,T)$ is the scaled amplitude of the convection state under consideration. Equation (1.2) includes Eqs. (1.1a) and (1.1b) near the CTP as special cases, leading to relations between the respective coefficients. Via these relations we are able to calculate the coefficients of Eq. (1.2) from those of Eqs. (1.1a) and (1.1b). The linear properties of Eq. (1.2) have been discussed in the context of binary fluid convection in Ref. [25] and parts of our results on the nonlinear coefficients f_1, f_2, and f_3 have been published in Ref. [49].

Close to a bifurcation point, the system becomes very sensitive to perturbations; thus a problem of fundamental interest is the influence of thermal fluctuations on the transition from the heat-conducting to the convecting state. Near phase transitions in thermodynamic equilibrium, thermal fluctuations induce a huge variety of interesting phenomena [50], but early calculations [51–53] for Rayleigh-Bénard convection have shown that here the influence of thermal noise on the threshold should usually be restricted to an experimentally unresolvable small range of the Rayleigh number [54]. Nevertheless, the effect of thermal fluctuations has been detected directly very recently in electroconvection of nematic liquid crystals [55] and, using an intrinsic amplification mechanism, also in binary fluid convection [18]. Theoretically the fluctuations can be described by adding a stochastic term to the amplitude equation, as has been done by Graham for the case of the stationary bifurcation in simple fluids with unrealistic (free) boundary conditions [52]. Here we extend these calculations to the Hopf bifurcation leading to the amplitude equation

$$\tau_0(\partial_t - v_g\partial_x)A = \epsilon(1+ic_0)A + \xi_0^2(1+ic_1)\partial_x^2 A - (\alpha+ic_2)|A|^2 A + \sqrt{Q}F(x,t) , \quad (1.3)$$

with the space-time correlation of the noise term given by

$$\langle F^*(x,t)F(x+\Delta x, t+\Delta t)\rangle = \delta(\Delta x)\delta(\Delta t)$$

and $\sqrt{Q}$ being the noise strength [52].

The paper is organized as follows. In Sec. II the basic equations and the boundary conditions are presented. Also, the method of solution and the linear stability analysis are given, as well as the derivation of the amplitude equations (1.1a) and (1.1b) from the basic equations, showing how the coefficients are calculated. Readers who are only interested in the results may omit this rather technical section, where the mathematical basis for the following is given, and should proceed directly to Secs. III, IV, or V. In Sec. III the results for the linear stability analysis are briefly outlined. We discuss in detail the coefficients of the amplitude equations for the stationary bifurcation, the traveling wave, and the standing waves. In Sec. IV the situation near the codimension-2 point is illustrated. We derive the coefficients of the amplitude equation (1.2) from the already-known coefficients of Eqs. (1.1a) and (1.1b) and discuss some important consequences. The influence of thermal fluctuations is considered in Sec. V, where we explicitly give the magnitude of the noise term appearing in Eq. (1.3) and compare it with the case of free, permeable boundary conditions. The quantitative agreement with recent experimental observations [18] is emphasized. Discussions of the results and, where possible, comparison with other calculations and experiments are presented at the end of Secs. III, IV, and V. Each of these sections may be read independently from the others.

II. BASIC EQUATIONS, METHOD OF SOLUTION AND AMPLITUDE EXPANSION

A. Hydrodynamic equations, heat-conduction state, and boundary conditions

We consider a binary fluid mixture in a gravitational field under the action of an external temperature gradient. The equations for the velocity $\mathbf{v}(\mathbf{r},t)$, the temperature $T(\mathbf{r},t)$, the concentration $N(\mathbf{r},t)$, and the pressure $p(\mathbf{r},t)$ describing the fluid behavior are, in Boussinesq approximation [8,9,56],

$$\nabla\cdot\mathbf{v}=0 , \quad (2.1a)$$

$$\frac{\partial T}{\partial t}+(\mathbf{v}\cdot\nabla)T=\kappa\nabla^2 T , \quad (2.1b)$$

$$\frac{\partial N}{\partial t}+(\mathbf{v}\cdot\nabla)N=D\left[\nabla^2 N+\frac{k_T}{T_0}\nabla^2 T\right] , \quad (2.1c)$$

$$\frac{\partial \mathbf{v}}{\partial t}+(\mathbf{v}\cdot\nabla)\mathbf{v}=-\frac{1}{\rho_0}\nabla p+\nu\nabla^2\mathbf{v}+\frac{\rho}{\rho_0}\mathbf{g} . \quad (2.1d)$$

Because the Dufour effect is negligible in fluid mixtures [8,9], the corresponding term is never included in this paper. Equation (2.1a) is the continuity equation for an incompressible fluid. In the heat equation (2.1b), κ is the thermal diffusivity of the fluid. In the continuity equation for the denser fluid component (2.1c), D is the solutional diffusivity and k_T is the Soret coefficient, which measures the cross coupling between temperature gradients and mass fluxes and can have either *plus* or *minus* sign. The momentum balance is described by the Navier-Stokes equations (2.1d) where ν is the kinematic viscosity of the fluid and the gravity field $\mathbf{g}$ is chosen parallel to the z direction: $\mathbf{g}=-g\mathbf{e}_z$. For the total density ρ, a linearized equation of state is used [8,9]:

$$\rho=\rho_0[1-\alpha(T-T_0)+\beta(N-N_0)] , \quad (2.2)$$

with $\alpha=-(1/\rho_0)\partial\rho/\partial T$ and $\beta=(1/\rho_0)\partial\rho/\partial N$.

We consider a horizontal fluid layer of infinite extent in the x-y plane with height d in z direction. At the confining top and bottom plates realistic (rigid and impervious) boundary conditions are assumed:

$$v_z=\frac{\partial v_z}{\partial z}=0=\frac{\partial N}{\partial z}+\frac{k_T}{T_0}\frac{\partial T}{\partial z} \quad \text{at } z=0,d ,$$
$$T=T_0+\Delta T \quad \text{at } z=0 , \quad (2.3)$$
$$T=T_0 \quad \text{at } z=d .$$

In contrast to unrealistic (free and pervious) boundary conditions, the vanishing tangential velocity components at the boundaries (*rigid*) lead to $\partial v_z/\partial z=0$ and the vanishing concentration flux (*impervious*) to $\partial N/\partial z+(k_T/T_0)\partial T/\partial z=0$ at $z=0,d$.

The conditions for stationary heat conduction without convective motion, $\mathbf{v}=\mathbf{0}$ and vanishing time derivatives, give for Eqs. (2.1a)–(2.1d) together with Eqs. (2.2) and (2.3) the solutions for the pure heat-conductive state:

$$T_{\rm cond}(z)=T_0+\Delta T\left[1-\frac{z}{d}\right], \tag{2.4a}$$

$$N_{\rm cond}(z)=N_0+\Delta N\left[1-\frac{z}{d}\right] \quad \text{with } \Delta N=-\frac{k_T}{T_0}\Delta T, \tag{2.4b}$$

$$\frac{\partial p_{\rm cond}}{\partial z}=-g\rho_0\left[1-(\alpha\Delta T-\beta\Delta N)\left[1-\frac{z}{d}\right]\right]. \tag{2.4c}$$

Here ΔN is not given by an explicit boundary condition as would be in the thermohaline problem [57], but through the Soret effect by the applied temperature difference.

Inserting $p(\mathbf{r},t)=p_{\rm cond}(z)+\delta p(\mathbf{r},t)$, $T(\mathbf{r},t)=T_{\rm cond}(z)+T'(\mathbf{r},t)$, and $N(\mathbf{r},t)=N_{\rm cond}(z)+N'(\mathbf{r},t)$ into Eqs. (2.1a)–(2.1d) eventually leads to the equations for the deviations from the heat-conduction state in dimensionless form (a two-dimensional, y-independent situation is assumed, because at the convection onset only two-dimensional rolls appear [3,8,9]):

$$\nabla\cdot\mathbf{u}=0, \tag{2.5a}$$

$$(\partial_t-\nabla^2)\vartheta-R\,\partial_x\Phi=(\partial_z\Phi\partial_x-\partial_x\Phi\partial_z)\vartheta, \tag{2.5b}$$

$$(\partial_t-L\nabla^2)\eta+\partial_t\vartheta-R\,\partial_x\Phi=(\partial_z\Phi\partial_x-\partial_x\Phi\partial_z)(\eta+\vartheta), \tag{2.5c}$$

$$(\partial_t\nabla^2-P\nabla^4)\Phi-P\Psi\partial_x\eta-P(1+\Psi)\partial_x\vartheta=(\partial_z\Phi\partial_x-\partial_x\Phi\partial_z)\nabla^2\Phi, \tag{2.5d}$$

with the boundary conditions

$$\Phi=\partial_z\Phi=\vartheta=\partial_z\eta=0 \quad \text{at } z=0,1. \tag{2.6}$$

Here lengths are scaled in units of layer thickness d and times in units of the thermal diffusion time d^2/κ, therefore the velocity is $\mathbf{v}=(\kappa/d)\mathbf{u}$. For the deviations of the temperature and the concentration field the scaling $T'=(\Delta T/R)\vartheta$ and $N'=-(k_T\Delta T/T_0R)c$ has been chosen. For convenience two new functions are introduced:

$$\eta(\mathbf{r},t):=c(\mathbf{r},t)-\vartheta(\mathbf{r},t), \tag{2.7a}$$

$$\Phi(\mathbf{r},t) \quad \text{with } u_z=\partial_x\Phi \text{ and } u_x=-\partial_z\Phi. \tag{2.7b}$$

With the so-defined *stream function* $\Phi(\mathbf{r},t)$, Eq. (2.5a) is fulfilled automatically. The pressure has been eliminated by mixing the x and z components of Eq. (2.1d), and we have set $\partial_\alpha f\equiv\partial f/\partial\alpha$ with $\alpha=x$, z, or t. The system is characterized by four dimensionless numbers, the *Prandtl number* P, the *Lewis number* L, the *Rayleigh number* R, and the *separation ratio* Ψ:

$$P=\frac{\nu}{\kappa}, \quad L=\frac{D}{\kappa}, \quad R=\frac{\alpha g d^3}{\kappa\nu}\Delta T, \quad \Psi=\frac{\beta k_T}{\alpha T_0}. \tag{2.8}$$

We consider P and L as fixed for a given fluid and shall use R and Ψ as two independent control parameters.

B. Linear stability of the heat-conduction state

For calculating the characteristics of the convection onset (e.g., the critical Rayleigh number, wave number, and frequency) from the underlying fluid equations two different methods have been used [19,24,25,28]. The set of ordinary linear differential equations appearing here (see below) was treated in the first approach by using analytically known independent fundamental solutions. This leads then in principle to the *exact linear solutions* [24,25]. For the second method a set of linearly independent solutions was calculated by numerical integration of the linearized fluid equations [19,28]. In both cases the factors for superposing these independent solutions are determined by fulfilling the boundary conditions. Even in the first case this step has to be done numerically. While the first approach provides a faster numerical code, the second one is more advantageous in view of the weakly nonlinear expansion. The first approach is already extensively described in [24,25], therefore we describe only the second one here.

For calculating the linear stability of the heat-conduction state, we only need the linear parts [left-hand sides (lhs's)] of Eqs. (2.5b)–(2.5d). The x and t dependences are separated out by the ansatz

$$\begin{bmatrix}\vartheta(x,z,t)\\ \eta(x,z,t)\\ \Phi(x,z,t)\end{bmatrix}=\begin{bmatrix}\vartheta_0(z)\\ \eta_0(z)\\ \dfrac{1}{ik}\Phi_0(z)\end{bmatrix}e^{ikx}e^{\sigma t}\equiv\hat{\mathbf{u}}_0(z)e^{ikx}e^{\sigma t}, \tag{2.9}$$

leading to the coupled ordinary differential equations

$$\vartheta_0''=(\sigma+k^2)\vartheta_0-R\Phi_0, \tag{2.10a}$$

$$\eta_0''=\left[\frac{\sigma}{L}+k^2\right]\eta_0+\frac{\sigma}{L}\vartheta_0-\frac{R}{L}\Phi_0, \tag{2.10b}$$

$$\Phi_0^{IV}=\left[\frac{\sigma}{P}+2k^2\right]\Phi_0''-k^2\left[\frac{\sigma}{P}+k^2\right]\Phi_0+\Psi k^2\eta_0+(1+\Psi)k^2\vartheta_0, \tag{2.10c}$$

with the abbreviations $f':=\partial f/\partial z$, $f'':=\partial^2 f/\partial z^2$, etc. With eight newly defined functions $y_1=\vartheta_0$, $y_2=\eta_0'$, $y_3=\Phi_0$, $y_4=\Phi_0'$, $y_5=\Phi_0''$, $y_6=\Phi_0'''$, $y_7=\vartheta_0'$, and $y_8=\eta_0$, Eqs. (2.10a)–(2.10c) can be written as an eight-dimensional system of first-order differential equations:

$$y_1'=y_7, \tag{2.11a}$$

$$y_2'=\frac{\sigma}{L}y_1-\frac{R}{L}y_3+\left[\frac{\sigma}{L}+k^2\right]y_8, \tag{2.11b}$$

$$y_3'=y_4, \tag{2.11c}$$

$$y_4'=y_5, \tag{2.11d}$$

$$y_5'=y_6, \tag{2.11e}$$

$$y_6' = (1+\Psi)k^2 y_1 - k^2\left[\frac{\sigma}{P}+k^2\right]y_3 + \left[\frac{\sigma}{P}+2k^2\right]y_5 + \Psi k^2 y_8 \ , \tag{2.11f}$$

$$y_7' = (\sigma+k^2)y_1 - R y_3 \ , \tag{2.11g}$$

$$y_8' = y_2 \ , \tag{2.11h}$$

and the boundary conditions following from Eq. (2.6) are

$$y_1 = y_2 = y_3 = y_4 = 0 \quad \text{at } z=0,1 \ . \tag{2.12}$$

With $\mathbf{y}$ being the eight-dimensional vector $(y_1(z), y_2(z), \ldots, y_8(z))$, $\mathbf{e}_i$ the eight 8-dimensional Cartesian unit vectors, and $\boldsymbol{\phi}_i$ and eight linear independent solutions of (2.11a)–(2.11h) with $\boldsymbol{\phi}_i(0)=\mathbf{e}_i$, the general solution is

$$\mathbf{y}(z) = \sum_{i=1}^{8} \alpha_i \boldsymbol{\phi}_i(z) \ . \tag{2.13}$$

The boundary conditions (2.12) at $z=0$ lead to $\alpha_1=\alpha_2=\alpha_3=\alpha_4=0$ so that (2.13) is reduced to $\mathbf{y}(z)=\sum_{i=5}^{8}\alpha_i\boldsymbol{\phi}_i(z)$.

Numerical integration (e.g., Runge-Kutta) of Eqs. (2.11a)–(2.11h) with the initial conditions $\mathbf{e}_5, \mathbf{e}_6, \mathbf{e}_7, \mathbf{e}_8$ at $z=0$ gives $\boldsymbol{\phi}_5(1), \boldsymbol{\phi}_6(1), \boldsymbol{\phi}_7(1), \boldsymbol{\phi}_8(1)$ and the resulting solution $\mathbf{y}(1)=\sum_{i=5}^{8}\alpha_i\boldsymbol{\phi}_i(1)$. The four parameters α_i have to be chosen such that the boundary conditions (2.12) at $z=1$ are fulfilled. This yields a set of homogeneous linear equations for the α_i (the superscripts denote the components of $\boldsymbol{\phi}_i$):

$$\begin{bmatrix} \phi_5^1(1) & \phi_6^1(1) & \phi_7^1(1) & \phi_8^1(1) \\ \phi_5^2(1) & \phi_6^2(1) & \phi_7^2(1) & \phi_8^2(1) \\ \phi_5^3(1) & \phi_6^3(1) & \phi_7^3(1) & \phi_8^3(1) \\ \phi_5^4(1) & \phi_6^4(1) & \phi_7^4(1) & \phi_8^4(1) \end{bmatrix} \begin{bmatrix} \alpha_5 \\ \alpha_6 \\ \alpha_7 \\ \alpha_8 \end{bmatrix} = \begin{bmatrix} 0 \\ 0 \\ 0 \\ 0 \end{bmatrix} , \tag{2.14}$$

with the solvability condition that the determinant of the coefficient matrix has to vanish: $\det(\cdots)=0$. This determinant is an implicit function, depending on $\sigma=s+i\omega$, k, and R as well as on the other dimensionless numbers ψ, P, and L, which we will consider fixed here. To make the structure of the linear stability calculation more transparent, we formally rewrite (2.14)

$$\det(\cdots) =: f(\sigma; k^2, R, \ldots) = 0 \tag{2.15}$$

with f being a real-valued function for $\omega=0$ and complex-valued otherwise $[f(\sigma^*)=f^*(\sigma)]$. Then for given values of k and R, σ has to be adjusted to fulfill Eq. (2.15), yielding the growth rate s and the frequency ω of the linear solution under consideration. To calculate the *neutral stability* defined by $s=0$, we now have to adjust R for a given k, again to fulfill Eq. (2.15). In other words, the condition $s=0$ gives us implicitly the *neutral curve* $R_0(k)$ and in the case of a Hopf bifurcation the frequency $\omega_0(k)$ on the neutral curve in addition. The convection onset is provided by the minimum of $R_0(k)$ giving the critical values $R_c=\min[R_0(k)]=R_0(k=k_c)$ and $\omega_c=\omega_0(k=k_c)$.

Now we can formulate the complete solution of the linear part of Eqs. (2.5b)–(2.5d) at threshold ($s=0$, R_c, k_c, and ω_c) as a superposition of four linear independent solutions (2.9) with $k=\pm k_c$ and $\omega=\pm\omega_c$:

$$\mathbf{u}_0(x,z,t) := \begin{bmatrix} \vartheta_0(x,z,t) \\ \eta_0(x,z,t) \\ \Phi_0(x,z,t) \end{bmatrix} = (A_0 e^{ik_c x} + B_0 e^{-ik_c x})\hat{\mathbf{u}}_0(z) e^{i\omega_c t} + \text{c.c.} \tag{2.16}$$

Here $\hat{\mathbf{u}}_0(z)$ is defined by Eq. (2.9), c.c. denotes the complex conjugate, and A_0 and B_0 are the amplitudes of the left and the right traveling waves, respectively. For the stationary bifurcation we have $\omega_c=0$ and one may set $B_0=0$.

To get unambiguous values for the nonlinear coefficients one needs a definite normalization of the linear solution. We choose $\mathbf{u}_0$ in such a manner that $\int_0^1 |\Phi_0(z)|^2 dz = 1$, with $\Phi_0(z)$ from Eq. (2.9).

C. Amplitude equations

One aim of this paper is to derive an expression for the as yet undetermined amplitudes A_0 and B_0 of Eq. (2.16), namely, the amplitude equations (1.1a) and (1.1b). The nonlinear coefficients of those equations determine the bifurcation behavior (subcritical or supercritical) and in the case of a supercritical bifurcation the absolute values of the amplitudes A_0 and B_0 up to first order in $\epsilon^{1/2}$, where ϵ measures the distance from threshold:

$$\epsilon := \frac{R-R_c}{R_c} \ . \tag{2.17}$$

We give in the following the general derivation for the Hopf bifurcation. The case of the stationary bifurcation is obtained by simply setting $B_0=0$ and $\omega=0$.

1. *Weakly nonlinear expansion of the basic equations*

We describe here the formal scheme for the derivation of the amplitude equations (1.1a) and (1.1b) following Refs. [34,39]. First we rewrite Eqs. (2.5b)–(2.5d) in the symbolic form

$$(\mathcal{M}\partial_t + \mathcal{L})\mathbf{u} = \mathbf{N}(\mathbf{u},\mathbf{u}) \ , \tag{2.18}$$

with $\mathbf{u}$ consisting of the fields ϑ, η, Φ and $\mathcal{M}$ and $\mathcal{L}$ representing the linear and $\mathbf{N}$ the nonlinear parts of Eqs. (2.5b)–(2.5d):

$$\mathbf{u}=\begin{bmatrix}\vartheta\\ \eta\\ \Phi\end{bmatrix},$$

$$\mathbf{N}=(\partial_z\Phi\partial_x-\partial_x\Phi\partial_z)\begin{bmatrix}\vartheta\\ \eta+\vartheta\\ \nabla^2\Phi\end{bmatrix},$$

$$\mathcal{M}=\begin{bmatrix}1&0&0\\ 1&1&0\\ 0&0&\nabla^2\end{bmatrix}, \tag{2.19}$$

$$\mathcal{L}=\begin{bmatrix}-\nabla^2 & 0 & -R\partial_x\\ 0 & -L\nabla^2 & -R\partial_x\\ -P(1+\Psi)\partial_x & -P\Psi\partial_x & -P\nabla^4\end{bmatrix}.$$

The amplitudes A_0 and B_0 now vary on the slow scales

$$X=\epsilon^{1/2}x\ ,\quad T_1=\epsilon^{1/2}t\ ,\quad T=\epsilon t\ , \tag{2.20}$$

which are treated as independent variables, so we have

$$A_0=A_0(X,T_1,T)\ \text{ and }\ B_0=B_0(X,T_1,T)\ . \tag{2.21}$$

We expand the solution of (2.18) with respect to $\epsilon^{1/2}$,

$$\mathbf{u}(x,z,t,X,T_1,T)=\epsilon^{1/2}\mathbf{u}_0(\cdots)+\epsilon\mathbf{u}_1(\cdots)+\epsilon^{3/2}\mathbf{u}_2(\cdots)+\cdots\ , \tag{2.22}$$

where the arguments on the left-hand side are repeated on the right-hand side, and substitute $\partial_t\to\partial_t+\epsilon^{1/2}\partial_{T_1}+\epsilon\partial_T$, $\partial_x\to\partial_x+\epsilon^{1/2}\partial_X$ according to Eq. (2.20) as well as $R=R_c(1+\epsilon)$. Inserting all this into Eq. (2.18) yields at successive orders of $\epsilon^{1/2}$

$$(\mathcal{M}\partial_t+\mathcal{L}_0)\mathbf{u}_0=0\quad(\epsilon^{1/2})\ , \tag{2.23a}$$

$$(\mathcal{M}\partial_t+\mathcal{L}_0)\mathbf{u}_1=\overline{\mathbf{N}}_1(\mathbf{u}_0)-(\mathcal{M}\partial_{T_1}+\overline{\mathcal{L}}_1)\mathbf{u}_0\quad(\epsilon)\ , \tag{2.23b}$$

$$(\mathcal{M}\partial_t+\mathcal{L}_0)\mathbf{u}_2=\overline{\mathbf{N}}_2(\mathbf{u}_0,\mathbf{u}_1)-\mathcal{M}(\partial_{T_1}\mathbf{u}_1+\partial_T\mathbf{u}_0)-\overline{\mathcal{L}}_2(\mathbf{u}_0,\mathbf{u}_1)\quad(\epsilon^{3/2})\ . \tag{2.23c}$$

The new operators $\overline{\mathcal{L}}_1,\overline{\mathcal{L}}_2$ and $\overline{\mathbf{N}}_1,\overline{\mathbf{N}}_2$ are complicated functions of the new variables, but we shall see below that it is not necessary to know their explicit form. $\mathcal{L}_0$ is the linear operator $\mathcal{L}$ defined in Eq. (2.19) with R replaced by R_c, so Eq. (2.23a) is simply the linear part of Eq. (2.18) with the already known solution (2.16), but where the amplitudes are now functions of the slow variables [see Eq. (2.21)]. The right-hand side (rhs) of Eq. (2.23b) depends only on $\mathbf{u}_0$, which is already calculated at order $\epsilon^{1/2}$ and is of the form of Eq. (2.16). Therefore Eq. (2.23b) is an inhomogeneous boundary-value problem for $\mathbf{u}_1(x,z,t,X,T_1,T)$ that can be solved by an integration scheme similar to the one described above. After inserting $\mathbf{u}_0$ and $\mathbf{u}_1$ into Eq. (2.23c), there is no need to really solve this equation. Projecting instead the whole equation onto $\mathbf{u}_0^\dagger$, where $\mathbf{u}_0^\dagger$ is the solution to the adjoint equation of (2.23a), the rhs of Eq. (2.23c) yields a solvability condition. By rescaling now back to the old variables x and t [and choosing a slightly different form of the expansion (2.22), where the factor $\epsilon^{1/2}$ is included into $\mathbf{u}_0$], these solvability conditions are the amplitude equations for A_0 and B_0, Eqs. (1.1a) and (1.1b).

Although the scheme of the above expansion is straightforward and in principle feasible, it would be a tremendous task to actually calculate the solution of the full Eq. (2.23b) and evaluate the inhomogeneous part of Eq. (2.23c). The procedure, however, can technically be performed much easier by calculating the linear and nonlinear coefficients of the amplitude equations separately, and this is described in the following section.

2. *Linear coefficients of the amplitude equations*

To get the linear coefficients τ_0, v_g, c_0, ξ_0^2, c_1 of Eqs. (1.1a) and (1.1b) one only needs to know the linear properties near R_c and k_c: the growth rate $s(R,k=k_c)$, the neutral curve $R_0(k)$, and the dispersion $\omega(k)$, so the nonlinear expansion is not necessary for this step. The derivation is given in detail in Ref. [39]. It is valid for many different systems, because it does not depend on the special form of the basic equations. Eventually one gets the following results [39]:

$$v_g=\frac{\partial\omega}{\partial k}\ ,\quad \tau_0=\frac{1}{R_c\dfrac{\partial s}{\partial R}}\ ,\quad c_0=R_c\tau_0\frac{\partial\omega}{\partial R}\ ,$$
$$\xi_0^2=\frac{1}{2R_c}\frac{\partial^2R}{\partial k^2}\ ,\quad c_1=-\frac{\tau_0}{2\xi_0^2}\frac{\partial^2\omega}{\partial k^2}\ . \tag{2.24}$$

The derivatives are all taken at the critical values $R_c,k_c,\omega_c,s=0$. While τ_0 and c_0 can in principle be calculated according to Eq. (2.24), a more accurate approach is to use an integral expression involving the linear solutions $\mathbf{u}_0$ and $\mathbf{u}_0^\dagger$ [see Ref. [25]; note the misprint on the lhs of their Eq. (3.15)]:

$$\frac{\tau_0}{1+ic_0}=\frac{\int_0^1[\eta_0^{\dagger *}(\eta_0+\vartheta_0)+\vartheta_0^{\dagger *}\vartheta_0-\Phi_0^{\dagger *}(\partial_z^2-k_c^2)\Phi_0]dz}{R_c\int_0^1[(\eta_0^{\dagger *}+\vartheta_0^{\dagger *})\Phi_0]dz}\ . \tag{2.25}$$

3. *Nonlinear coefficients of the amplitude equations*

To calculate the nonlinear coefficients α, c_2, γ, c_3 of Eqs. (1.1a) and (1.1b) the introduction of the slow variables X and T is not necessary, because they only appear in the linear part of the amplitude equations, which is now known from Sec. II C 2. With this simplification one obtains instead of Eqs. (2.23a)–(2.23c)

$$(\mathcal{M}\partial_t+\mathcal{L}_0)\mathbf{u}_0=0\quad(\epsilon^{1/2})\ , \tag{2.26a}$$

$$(\mathcal{M}\partial_t+\mathcal{L}_0)\mathbf{u}_1=\mathbf{N}_1(\mathbf{u}_0)\quad(\epsilon)\ , \tag{2.26b}$$

$$(\mathcal{M}\partial_t+\mathcal{L}_0)\mathbf{u}_2=\mathbf{N}_2(\mathbf{u}_0,\mathbf{u}_1)-\mathcal{L}_2\mathbf{u}_0\quad(\epsilon^{3/2})\ , \tag{2.26c}$$

where the operators $\mathbf{N}_i$ and $\mathcal{L}_2$ are now simpler than those above in Eqs. (2.23b) and (2.23c). $\mathcal{L}_0$ is again the linear operator defined in Eq. (2.19) with R replaced by R_c and $\mathbf{N}_1(\mathbf{u}_0)$ is also given by Eq. (2.19) with the functions ϑ, η, and Φ replaced by ϑ_0, η_0, and Φ_0. The

remaining operators are

$$L_2=\begin{bmatrix}0 & 0 & -R_c\partial_x\\ 0 & 0 & -R_c\partial_x\\ 0 & 0 & 0\end{bmatrix}$$

and

$$\mathbf{N}_2(\mathbf{u}_0,\mathbf{u}_1)=(\partial_z\Phi_0\partial_x-\partial_x\Phi_0\partial_z)\begin{bmatrix}\vartheta_1\\ \eta_1+\vartheta_1\\ \nabla^2\Phi_1\end{bmatrix}+(\partial_z\Phi_1\partial_x-\partial_x\Phi_1\partial_z)\begin{bmatrix}\vartheta_0\\ \eta_0+\vartheta_0\\ \nabla^2\Phi_0\end{bmatrix}.$$

To facilitate the calculation further, the complete solution (2.16) is not inserted into Eq. (2.26b), but rather we consider the system (2.26a)–(2.26c) separately for the traveling waves ($B_0=0$) and for the standing waves ($A_0=B_0$). Then inserting $\mathbf{u}_0$ into (2.26b) again yields $\mathbf{u}_1$ and the solvability condition for Eq. (2.26c) now reads, after projecting onto $\hat{\mathbf{u}}_0^{\dagger}$,

$$0=-A_0\int_0^1\hat{\mathbf{u}}_0^{\dagger *}\delta\mathcal{L}_0\hat{\mathbf{u}}_0dz+|A_0|^2A_0\int_0^1\hat{\mathbf{u}}_0^{\dagger *}\hat{\mathbf{N}}_2dz$$
$$=:I_1A_0+I_2|A_0|^2A_0\ , \tag{2.27}$$

with $\hat{\mathbf{u}}_0$ defined by Eq. (2.16). $\hat{\mathbf{N}}_2$ is $\mathbf{N}_2$ from above with only the z dependence remaining and where also the amplitude factor A_0 has been drawn out. We have

$$\delta\mathcal{L}_0=\begin{bmatrix}0 & 0 & -R_c\\ 0 & 0 & -R_c\\ 0 & 0 & 0\end{bmatrix}.$$

The integrals I_1 and I_2 are calculated by using the explicit numerical expressions for $\mathbf{u}_0$ and $\hat{\mathbf{N}}_2$. Now comparing Eq. (2.27) with either Eqs. (1.1a) or (1.1b) (with no coupling terms, because only one wave is considered) one can identify

$$\alpha=\mathrm{Re}(\zeta)\ \text{ and }\ c_2=\mathrm{Im}(\zeta)\ \text{ with }\ \zeta=-(1+ic_0)\frac{I_2}{I_1}\ . \tag{2.28}$$

Doing this separately for the TW's and the SW's, we obtain $\alpha^{\mathrm{TW}},c_2^{\mathrm{TW}}$ as well as $\alpha^{\mathrm{SW}},c_2^{\mathrm{SW}}$ for the respective amplitude equations. To get from these the coefficients of the coupled amplitude equations (1.1a) and (1.1b) one has to extract the two special cases. For TW's ($B_0=0$) it is easy to see that

$$\alpha=\alpha^{\mathrm{TW}}\ \text{ and }\ c_2=c_2^{\mathrm{TW}}\ , \tag{2.29a}$$

while for the SW's ($A_0=B_0$) one gets for the nonlinear part of Eq. (1.1a)

$$-[\alpha+\gamma+i(c_2+c_3)]|A_0|^2A_0=:-(\alpha^{\mathrm{SW}}+ic_2^{\mathrm{SW}})|A_0|^2A_0$$

yielding

$$\gamma=\alpha^{\mathrm{SW}}-\alpha^{\mathrm{TW}}\ \text{ and }\ c_3=c_2^{\mathrm{SW}}-c_2^{\mathrm{TW}}\ . \tag{2.29b}$$

For the stationary pattern (SP) where $B_0=0$ the situation is much simpler, because only one equation arises and the whole procedure for deriving the remaining nonlinear coefficients has to be done only once.

III. CONVECTION ONSET AND COEFFICIENTS OF THE AMPLITUDE EQUATIONS: RESULTS

With the tools described in Sec. II the threshold properties, such as the critical Rayleigh number R_c, the critical wave number k_c, and the Hopf frequency ω_c, as well as the coefficients for the amplitude equations (1.1a) and (1.1b), can now be calculated for the stationary and the oscillatory bifurcation for different parameter combinations. We have chosen $L=0.03$, $P=0.6$, which is appropriate for a ^{3}He-^{4}He mixture [12] and $L=0.01$, $P=10$ for a water-ethanol mixture [14,16,18].

In order to test the numerical calculations we have compared R_c, k_c, and ω_c with the results of Refs. [24,25]. The linear coefficients of the amplitude equations for the Hopf bifurcation are given in Ref. [25] and for $\Psi=0$ the case of a simple fluid has to be recovered, where the nonlinear coefficient is known [35,58]. These values are all reproduced. Furthermore, for unrealistic (free and pervious) boundary conditions, where all coefficients can be calculated analytically, we obtain the correct results by the numerics. Another test for some linear and the nonlinear coefficients is their behavior near the codimension-2 point, where they have to fulfill some consistency relations (see Refs. [41,49] and Sec. IV below).

For further reference, we first discuss very briefly the linear stability behavior (for more details see Ref. [24]). Figure 1 shows the stability diagram for a fluid with $L=0.03$, $P=0.6$ for realistic boundary conditions. The critical Rayleigh numbers R_c^{stat} (solid line) and R_c^{osc} (dashed line) coincide at the CTP at

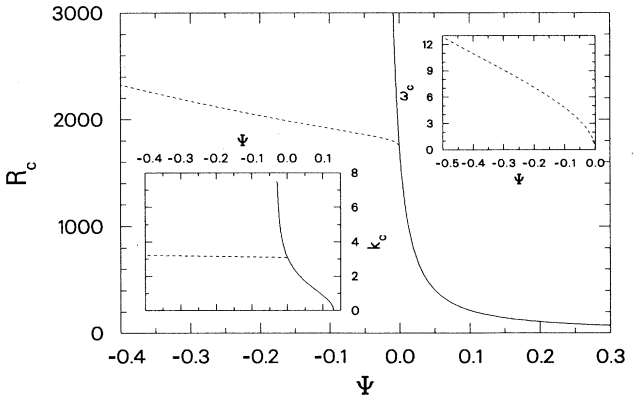

FIG. 1. Stability diagram for a fluid with $L=0.03$ and $P=0.6$. The solid and dashed lines represent the stationary and the oscillatory bifurcation, respectively. The curves for the critical Rayleigh number R_c intersect at slightly negative Ψ, at the codimension-2 point. The insets show the critical wave number k_c and the critical frequency ω_c as functions of Ψ.

$\Psi_{CTP} = -5.4346 \times 10^{-4}$. R_c^{osc} does not end at the CTP as for free boundary conditions, but exists in a small range for $\Psi > \Psi_{CTP}$. This has to do with the fact that the critical wave numbers k_c^{stat} for the stationary and k_c^{osc} for the oscillatory bifurcation are different at the CTP and the critical frequency is not zero there. R_c^{stat} diverges for slightly negative Ψ at Ψ_d, a value that can be given analytically for free, pervious boundaries: $\Psi_d = -L/(1+L)$. Here the characteristic polynomial of the basic equations (2.5b)–(2.5d) becomes highly degenerate, which leads to the fact that R_c^{stat} for realistic boundary conditions diverges at the same Ψ_d and the critical wave number k_c^{stat} reaches a value independent of L.

The critical wave number k_c^{osc} for the Hopf bifurcation stays nearly constant over the whole Ψ regime, while k_c^{stat} decreases rapidly for positive Ψ and becomes zero for $\Psi > \Psi_\infty \approx 0.13$ (see lower left inset of Fig. 1). This feature of infinite wavelength has been discussed in detail in Refs. [24,57] and the value of Ψ_∞ can be given analytically: $\Psi_\infty = L/(\frac{34}{131} - L)$ and $R_c = 720L/\Psi$ for $\Psi > \Psi_\infty$ [24]. The upper right inset in Fig. 1 shows the critical frequency ω_c.

A. Stationary bifurcation

The linear solution at threshold (2.16) simplifies for the stationary pattern (SP) to

$$\mathbf{u}_0(x,z) = A_0 \hat{\mathbf{u}}_0(z) e^{ik_c x} + \text{c.c.} , \tag{3.1}$$

leading to the amplitude equation for A_0,

$$\tau_0 \partial_t A_0 = \epsilon A_0 + \xi_0^2 \partial_x^2 A_0 - \alpha |A_0|^2 A_0 . \tag{3.2}$$

In Fig. 2 we give the coefficients of Eq. (3.2) as functions of Ψ for $L = 0.03$, $P = 0.6$ (solid lines) and $L = 0.01$, $P = 10$ (dashed lines). It is worth mentioning that for the stationary bifurcation R_c, k_c, and ξ_0^2 depend only on L, whereas τ_0 and α depend on L and P. For $\Psi = 0$ only the P dependence is left.

The coherence length ξ_0, shown in Fig. 2(a), tends to zero for $\Psi \to \Psi_\infty$, where the neutral curve becomes flatter and flatter. The maximum value of ξ_0^2 for negative Ψ is independent of L, but not the locations of these points. For $\Psi \to \Psi_d$, ξ_0^2 seems to have a nonzero value, which is independent of L. The relaxation time τ_0 shown in Fig. 2(b) diverges for $\Psi = \Psi_\infty$. The blowup near $\Psi = 0$ (see inset) shows that τ_0 depends on P for $\Psi = 0$ (dotted line) and we found $\tau_0 \propto 1/P$ for small P (as for unrealistic boundary conditions). This dependence is also known from calculations for a simple fluid with realistic boundaries [35]. τ_0 crosses zero for Ψ slightly smaller than Ψ_{CTP}, while for free, previous boundaries one has $\tau_0(\Psi_{CTP}) = 0$.

Finally, the nonlinear coefficient α is given in Fig. 2(c). For $\Psi > 0$ it is positive, so here we deal with a forward bifurcation. α diverges for $\Psi = \Psi_\infty$, indicating that the amplitude A_0 tends to zero. At this point the linear solution (3.1) ceases to exist. For $\Psi = 0$, α depends on P (in contrast to unrealistic boundaries, where $\alpha = \text{const}$), but the influence is noticeable only for $P < 0.2$. This can be seen from Fig. 3, where $\alpha(\Psi = 0)$ is plotted against P. We

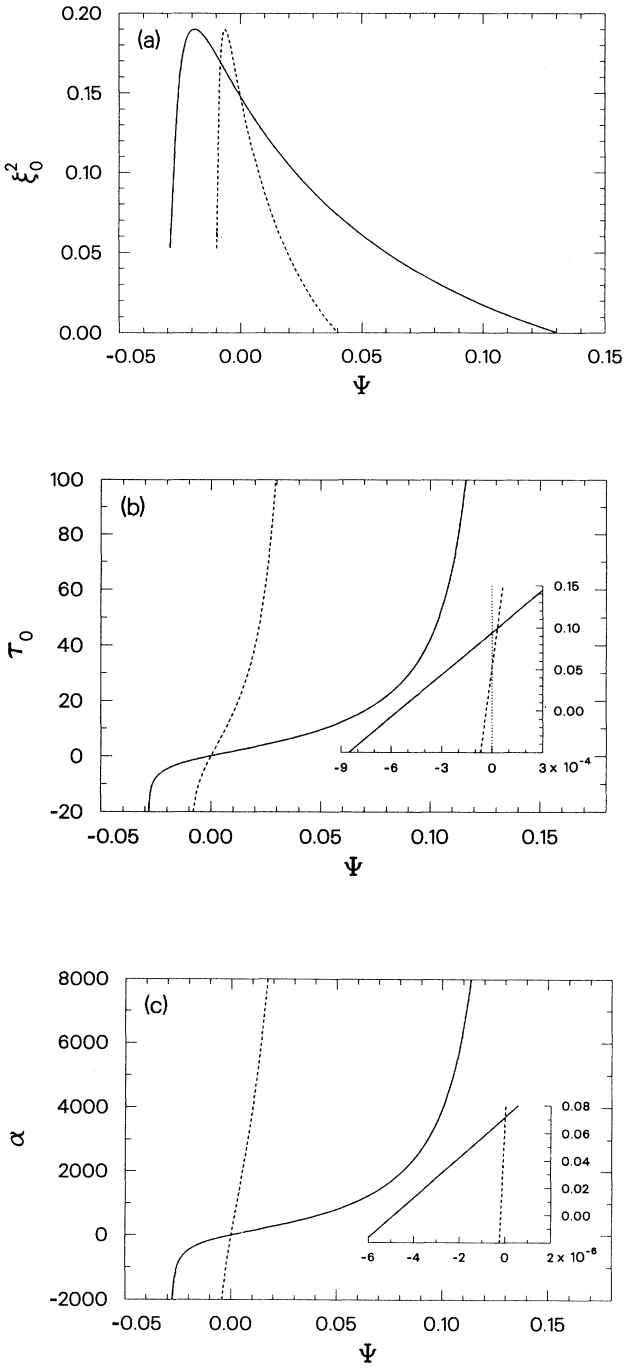

FIG. 2. Coefficients of the amplitude equation (3.1) as functions of Ψ for $L = 0.03$, $P = 0.6$ (solid line) and $L = 0.01$, $P = 10$ (dashed line). (a) The coherence length ξ_0^2 tends to zero for $\Psi = \Psi_\infty$, where k_c becomes zero and therefore the wavelength diverges (see lower inset of Fig. 1). (b) The relaxation time τ_0 diverges for $\Psi = \Psi_\infty$. The inset is an extreme magnification of the regime near $\Psi = 0$. $\Psi = 0$ is indicated by the dotted line. τ_0 changes sign for $\Psi < \Psi_{CTP}$. (c) The nonlinear coefficient α diverges for $\Psi = \Psi_\infty$. The inset is an extreme magnification of the regime near $\Psi = 0$. α changes sign at the tricritical point Ψ_{TC}^{stat}. For $\Psi > \Psi_{TC}^{stat}$ the bifurcation is forward; otherwise it is backward.

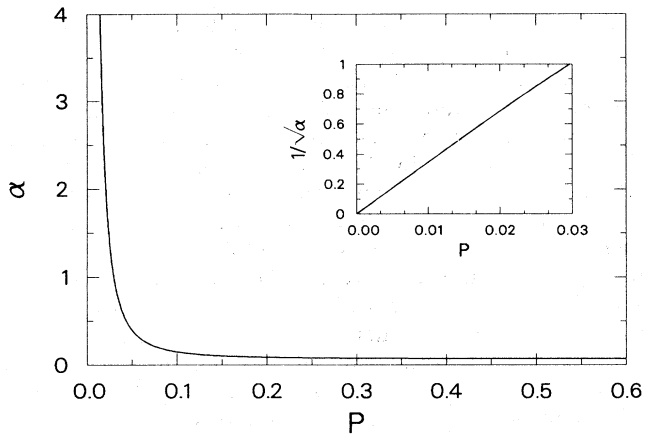

FIG. 3. Dependence of α on the Prandtl number P for $\Psi=0$. The influence is important only for $P<0.02$ and goes like $1/P^2$ for small P (see inset).

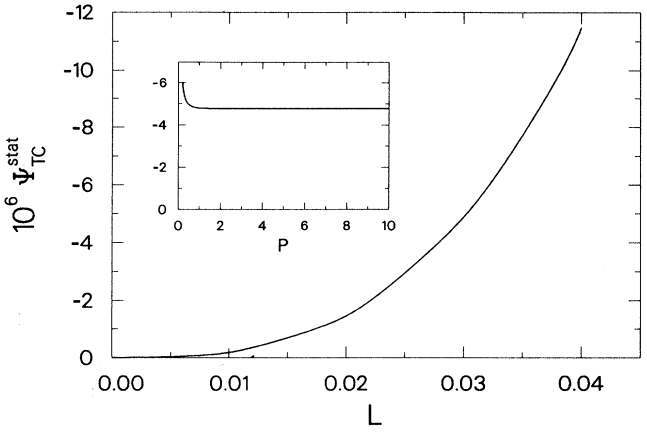

FIG. 4. Dependence of the tricritical point Ψ_{TC}^{stat} on L for fixed $P=0.6$, where the proportionality $\Psi_{TC}^{stat}\propto -L^3$ is found. The inset shows the dependence on P for fixed $L=0.03$. This influence is important only for $P<1$.

found $\alpha\propto 1/P^2$ for small P; see inset of Fig. 3 where we plotted $1/\sqrt{\alpha}$ vs P (see also Ref. [35]). The same relation holds for other values of Ψ with a noticeable influence restricted to still smaller values of P, so for usual fluids this P dependence is unimportant. α changes sign at the tricritical point at Ψ_{TC}^{stat} and for $\Psi<\Psi_{TC}^{stat}$ the bifurcation is subcritical. We always find $\Psi_{CTP}<\Psi_{TC}^{stat}<0$, so the bifurcation is backward at the CTP. In Fig. 4 we show the dependence of the location of the tricritical point on L for fixed $P=0.6$. The proportionality $\Psi_{TC}^{stat}\propto -L^3$ for small L agrees with the result obtained for free boundary conditions. The inset shows Ψ_{TC}^{stat} as a function of P for fixed $L=0.03$. Variations become important only for $P<1$ (for free boundary conditions Ψ_{TC}^{stat} does not depend on P).

In Table I we give the numerical values of the coefficients of Eq. (3.2) for our parameters P and L for three different values of Ψ. We have chosen the codimension-2 point Ψ_{CTP}, $\Psi=0$ and a positive value $\Psi\approx\Psi_\infty/2$. The critical values R_c and k_c are listed, too.

B. Hopf bifurcation

Since we are discussing the TW's and the SW's separately, we can consider a single amplitude equation having the same form for both cases:

$$\tau_0\partial_t A_0=\epsilon(1+ic_0)A_0+\xi_0^2(1+ic_1)\partial_x^2 A_0 -(\alpha+ic_2)|A_0|^2A_0\ . \tag{3.3}$$

For this purpose, for TW's, we have transformed into the comoving frame ($x\rightarrow x\pm v_g t$) and for SW's we have set $A_0=B_0$. The linear coefficients given by Eqs. (2.24) and (2.25) are equal in both cases and are discussed in detail in Ref. [25]. These results are compatible with ours except for c_1 for small $|\Psi|$ values. Here we have improved our numerical accuracy leading to a correction of our former results on c_1 [28].

According to Eq. (2.24) one has to differentiate numerically the function $\omega(k)$ by evaluating $\omega(k_c\pm n\Delta k)$ at different values of the wave number k, depending on the order of the formula for the derivative ($n=0,1,2,\ldots$). It has turned out that the result depends on the choice of Δk and we have to find the optimal Δk_0 using the method described in Ref. [59] (see Fig. 1 therein). This Δk_0 depends on Ψ. In Fig. 5 we show as a result of these sophisticated calculations c_1 as a function of Ψ for $L=0.03$, $P=0.6$. In most of the Ψ regime there is no qualitative change to the former results and c_1 changes sign for $\Psi<\Psi_{CTP}$ (here at $\Psi=-0.105$). The remarkable feature not discussed before is shown in the inset of Fig. 5

TABLE I. Coefficients of the amplitude equation (3.2) and the critical values for three different Ψ: Ψ_{CPT}, $\Psi=0$, and $\Psi\approx\Psi_\infty/2$.

	$\Psi=$	$L=0.01$, $P=10$ $\Psi_{CTP}=-3.526\times10^{-5}$			$L=0.03$, $P=0.6$ $\Psi_{CTP}=-5.4346\times10^{-4}$		
Coeff.		Ψ_{CTP}	0	0.02	Ψ_{CTP}	0	0.06
R_c		1717.27	1707.76	347.90	1758.26	1707.76	346.43
k_c		3.1216	3.1163	1.4817	3.1435	3.1163	1.5245
ξ_0^2		0.148	0.148	0.048	0.149	0.148	0.050
τ_0		1.93×10^{-4}	0.0535	39.67	0.0024	0.0943	12.46
α		−13.75	0.0701	10404	−7.95	0.0716	1082

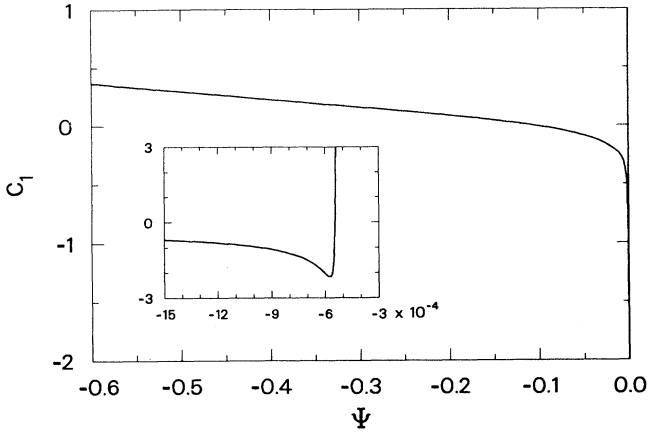

FIG. 5. Linear coefficient c_1 of the amplitude equation (3.3) as a function of Ψ for $L=0.03$, $P=0.6$. The inset is a magnification of the regime near the codimension-2 point. c_1 changes sign very close to the CTP.

and happens near the CTP. After the sign change, c_1 reaches a minimum and increases again for increasing Ψ, going through zero not exactly at, but very close to the CTP, namely, at $\Psi=-5.44\times10^{-4}$ ($\Psi_{\rm CTP}=-5.4346\times10^{-4}$). This is consistent with the degenerate amplitude equation (1.3) valid near the CTP (see Ref. [41] and Sec. IV).

From now on we regard only the nonlinear coefficients of Eq. (3.3), which have to be derived individually for the TW's and the SW's. For $\alpha>0$, Eq. (3.3) has the periodic solution

$$A_0(x,t)=\left[\frac{\epsilon}{\alpha}\right]^{1/2}F\exp\left[i\left[K\frac{x}{\xi_0}+\Omega\frac{t}{\tau_0}\right]\right], \qquad (3.4)$$

with $F^2=1-K^2/\epsilon$, and $\Omega=\epsilon[c_0-(c_2/\alpha)]-[c_1-(c_2/\alpha)]K^2$. These solutions are stable in a finite wave-number band if $\alpha+c_1c_2>0$. Otherwise Benjamin-Feir instability arises and the solution is unstable in the whole range of existence $K^2<\epsilon$ [34]. If the bifurcation is forward for TW's as well as for SW's, then for $\alpha^{\rm SW}>2\alpha^{\rm TW}$ the TW's are stable with respect to periodic perturbations [42]. We shall see below that for $\alpha^{\rm TW}>0$ this is always the case. If one of the coefficients $\alpha^{\rm SW}$ or $\alpha^{\rm TW}$ is less than zero, the bifurcation is backward and the solution (3.4) becomes unstable. There still exist, however, stable small-amplitude chaotic and even stationary solutions in some range of the c_1-c_2 regime [47]. For more general large-amplitude solutions near $\Psi_{\rm TC}$ an amplitude equation up to fifth order has to be derived, while further away from $\Psi_{\rm TC}$, $\Psi<\Psi_{\rm TC}$, only the full numerics seems to be a reasonable approach.

1. *Traveling waves*

For, e.g., a left TW ($B_0=0$) the linear solution (2.16) becomes

$$\mathbf{u}_0(x,z,t)=A_0\hat{\mathbf{u}}_0(z)e^{i(k_cx+\omega_ct)}+\text{c.c.} \qquad (3.5)$$

and the whole procedure described in Sec. II C 3 has to be done with this expression, eventually leading to the nonlinear coefficients $\alpha^{\rm TW}$ and $c_2^{\rm TW}$ of Eq. (3.3). The results are plotted as functions of Ψ in Fig. 6 for $L=0.03$, $P=0.6$ (dot-dashed lines) and $L=0.01$, $P=10$ (dashed lines). $\alpha^{\rm TW}$, shown in Fig. 6(a), is negative in nearly the whole Ψ regime. So the bifurcation is in most cases backward, a fact that was already known from early experiments in binary mixtures [9]. Only near $\Psi=0$, $\alpha^{\rm TW}$ changes sign and the bifurcation becomes forward (see inset). The location of this tricritical point $\Psi_{\rm TC}^{\rm TW}$ depends on the Lewis number L such as $-L^2$ for small L [see Fig. 8(a)], so for an exploration of this regime a fluid with large L would be desirable. At the CTP $\alpha^{\rm TW}$ is positive. The coefficient $c_2^{\rm TW}$, which determines the nonlinear frequency renormalization [see Eq. (3.4)], is shown in Fig. 6(b). It is positive over the whole Ψ regime and from the inset one sees that $c_2^{\rm TW}$ diverges for small absolute values of Ψ. This happens where the oscillatory branch ceases to exist.

For the question of Benjamin-Feir instability one has

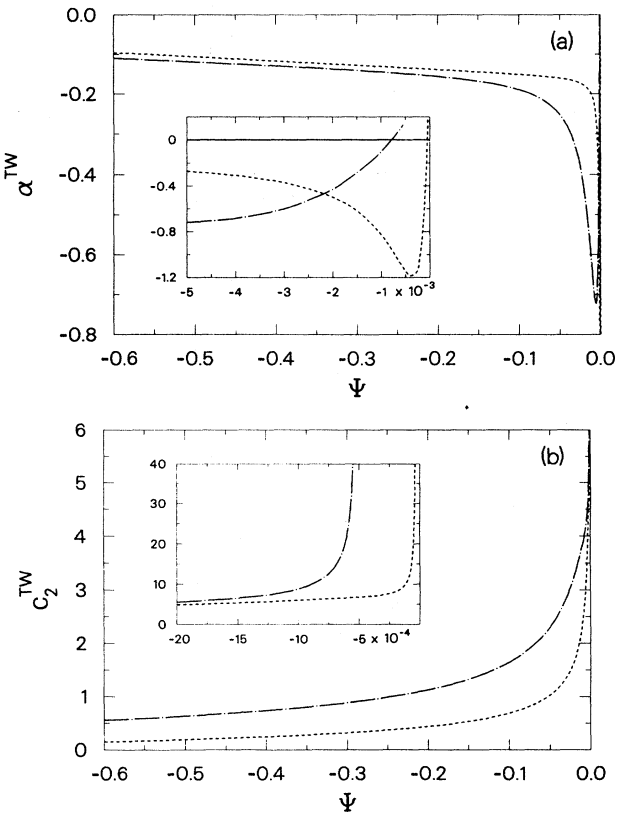

FIG. 6. Nonlinear coefficients for traveling waves for $L=0.03$, $P=0.6$ (dot-dashed lines) and $L=0.01$, $P=10$ (dashed lines). The insets are magnifications of the regime near $\Psi=0$. (a) $\alpha^{\rm TW}$ is negative in nearly the whole Ψ regime and changes sign only for very slightly negative Ψ (see inset). So the bifurcation is in most cases backward, but is forward at the codimension-2 point. (b) $c_2^{\rm TW}$ is always positive and diverges at that point where the oscillatory branch ends.

to calculate $\alpha^{TW}+c_1 c_2^{TW}$, which allows for stable TW's only for a positive value. In the case of forward bifurcating TW's ($\alpha^{TW}>0$) this quantity is negative except for a very small range near the CTP. For $L=0.03$, $P=0.6$, α^{TW} becomes positive at $\Psi_{TC}^{TW}=-7.858\times10^{-4}$, but the solution (3.4) is stable only for $-5.44\times10^{-4}<\Psi<\Psi_{CTP}$ with $\Psi_{CTP}=-5.4346\times10^{-4}$; otherwise it is unstable. This is consistent with the general investigation of the vicinity of the CTP (see Ref. [41] and Sec. IV below).

2. *Standing waves*

Here the linear solution can be constructed, e.g., by setting $A_0=B_0$ in Eq. (2.16), leading to

$$\mathbf{u}_0(x,z,t)=2A_0\hat{\mathbf{u}}_0(z)\cos(k_c x)e^{i\omega_c t}+\text{c.c.}\ , \tag{3.6}$$

and the expansion procedure of Sec. II C 3 yields α^{SW} and c_2^{SW} shown in Fig. 7 for the same parameters as above. α^{SW}, plotted in Fig. 7(a), can have one or three tricritical points. For our parameter combinations α^{SW} changes sign three times, but for $L=0.03$, $P=5$ this would happen only once. The tricritical points occur for small absolute values of Ψ, so α^{SW} is negative in most of the Ψ regime also. The inset shows a magnification of the regime near $\Psi=0$, indicating that the tricritical point for SW's, Ψ_{TC}^{SW}, always lies below Ψ_{TC}^{TW}. In the range where the bifurcations for TW's and for SW's are both forward, we found $\alpha^{SW}>2\alpha^{TW}$, leading to TW's in this regime. The coefficient c_2^{SW}, shown in Fig. 7(b), has a similar behavior as c_2^{TW}. It is always positive and diverges where the oscillatory branch ends. This is also consistent with the more general considerations of Sec. IV.

3. *Coupled amplitude equations*

To describe the near-threshold behavior in the case of a Hopf bifurcation in general, the coupled amplitude equations (1.1a) and (1.1b) have to be considered, whose coefficients can now all be given. The linear ones are those from Eq. (2.24); α and c_2 are simply α^{TW} and c_2^{TW} given in Fig. 6. With α^{SW} and c_2^{SW} from Fig. 7, it is easy to calculate γ and c_3 according to Eq. (2.29b). The results are shown in Fig. 8(a) (γ) and 8(b) (c_3) for the same parameters as above.

In Table II we give the full set of the coefficients of

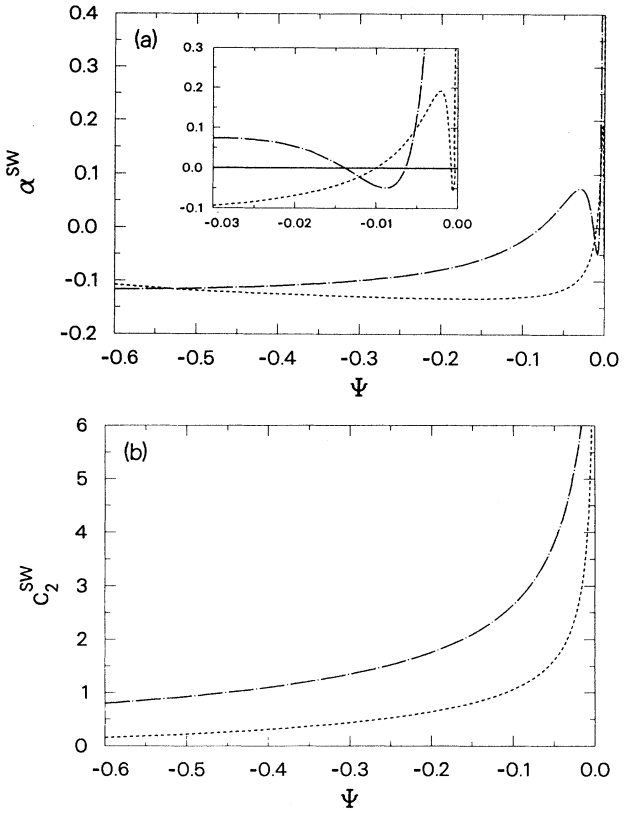

FIG. 7. Nonlinear coefficients for standing waves for $L=0.03$, $P=0.6$ (dot-dashed lines) and $L=0.01$, $P=10$ (dashed lines). (a) In contrast to α^{TW}, α^{SW} changes sign up to three times, but is also negative in a large range of the Ψ regime. The behavior near $\Psi=0$ is shown in the inset. α^{SW} is positive at the codimension-2 point. (b) c_2^{SW} is always positive and diverges where the oscillatory branch ends.

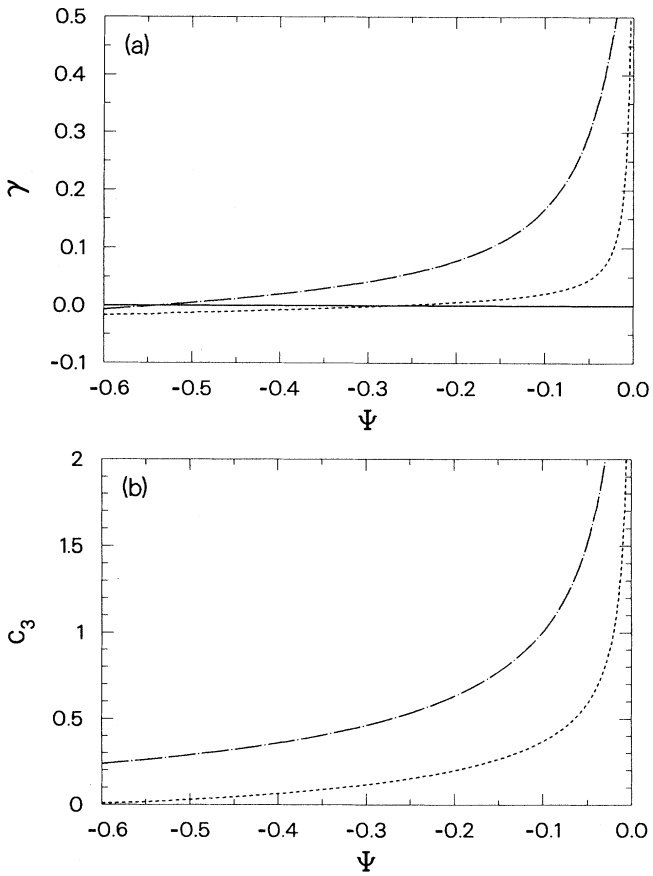

FIG. 8. The remaining nonlinear coefficients for the coupled amplitude equations (1.1a) and (1.1b) for $L=0.03$, $P=0.6$ (dot-dashed lines) and $L=0.01$, $P=10$ (dashed lines). (a) $\gamma=\alpha^{SW}-\alpha^{TW}$. (b) $c_3=c_2^{SW}-c_2^{TW}$.

TABLE II. Coefficients of the amplitude equations (1.1a) and (1.1b) and the critical values for different Ψ: Ψ_{CTP}, Ψ_{TC}^{TW}, $\Psi=-0.1$, and $\Psi=-0.5$.

	$\Psi=$	$L=0.01$, $P=10$ $\Psi_{CTP}=-3.526\times10^{-5}$ $\Psi_{TC}^{TW}=-5\times10^{-5}$			$L=0.03$, $P=0.6$ $\Psi_{CTP}=-5.4346\times10^{-4}$ $\Psi_{TC}^{TW}=-7.858\times10^{-4}$			
Coeff.		Ψ_{TC}^{TW}	-0.1	-0.5	Ψ_{CTP}	Ψ_{TC}^{TW}	-0.1	-0.5
R_c		1717.53	1912.79	3347.49	1758.26	1759.83	1916.44	2498.69
k_c		3.1103	3.1231	3.1704	3.0754	3.0753	3.1210	3.2643
ω_c		0.0636	6.466	19.45	0.0460	0.1997	4.7997	12.85
τ_0		0.105	0.106	0.104	0.186	0.185	0.183	0.192
v_g		-0.027	2.004	5.89	-0.661	-0.101	1.231	3.023
c_0		-1.517	0.293	0.956	-6.059	-1.386	0.213	0.897
ξ_0^2		0.148	0.147	0.143	0.152	0.152	0.148	0.142
c_1		-1.5	0.071	0.319	0.26	-1.25	-0.006	0.296
α		9×10^{-5}	-0.151	-0.106	0.135	-1×10^{-5}	-0.190	-0.119
c_2		21.37	0.690	0.192	49.97	11.47	1.643	0.632
γ		13.59	0.021	-0.013	18.54	7.49	0.166	0.0047
c_3		26.10	0.368	0.029	94.34	13.99	1.002	0.288

Eqs. (1.1a) and (1.1b) together with the critical values R_c, k_c, and ω_c. For $L=0.03$, $P=0.6$ we have chosen the codimension-2 point Ψ_{CTP}, the tricritical point for traveling waves Ψ_{TC}^{TW}, and two more negative values $\Psi=-0.1$ and -0.5. For $L=0.01$, $P=10$ the CTP at $\Psi_{CTP}=-3.526\times10^{-5}$ lies outside our resolution for the nonlinear coefficients (here $\omega_{CTP}\approx0.006$ and numerical problems arise), so the results are given only for three values of Ψ.

C. Discussion

From the calculations of the coefficients of the amplitude equations (1.1a) and (1.1b) we found the bifurcation behavior and the locations of the tricritical points for the SP, the TW's, and the SW's. A codimension-2 bifurcation occurs for slightly negative $\Psi=\Psi_{CTP}<0$, separating the stationary bifurcation ($\Psi>\Psi_{CTP}$) from the Hopf bifurcation ($\Psi<\Psi_{CTP}$). At the CTP the TW's and the SW's bifurcate supercritically whereas the SP bifurcates subcritically. In Fig. 9 we give the locations of the CTP (solid lines) and of the tricritical points for the TW's Ψ_{TC}^{TW} (dashed lines) and for the SW's Ψ_{TC}^{SW} (dot-dashed lines) as functions of the material parameters. Figure 9(a) shows the dependencies on L for fixed $P=0.6$, where we found the proportionality $\Psi_{crit}\propto -L^2$ for small L. In Fig. 9(b) the dependencies on P for fixed $L=0.03$ are plotted. All three types of solutions, the SP, the TW's, and the SW's, show a transition from supercritical to subcritical very close to the CTP and we found $\Psi_{TC}^{SW}<\Psi_{TC}^{TW}<\Psi_{CTP}<\Psi_{TC}^{stat}<0$. For Lewis number $L\to0$ they all tend to zero as shown in Figs. 4 and 9(a). The TW's and SW's bifurcate subcritically in most of the range where the Hopf bifurcation comes first, while the SP shows a supercritical bifurcation in most of the range where the stationary bifurcation comes first. The normal-fluid $\Psi=0$ becomes a highly singular point for $L\to0$ and for small values of L one has a near degeneracy. Perhaps this scenario can be resolved experimentally using gas mixtures where L is of the order $O(1)$.

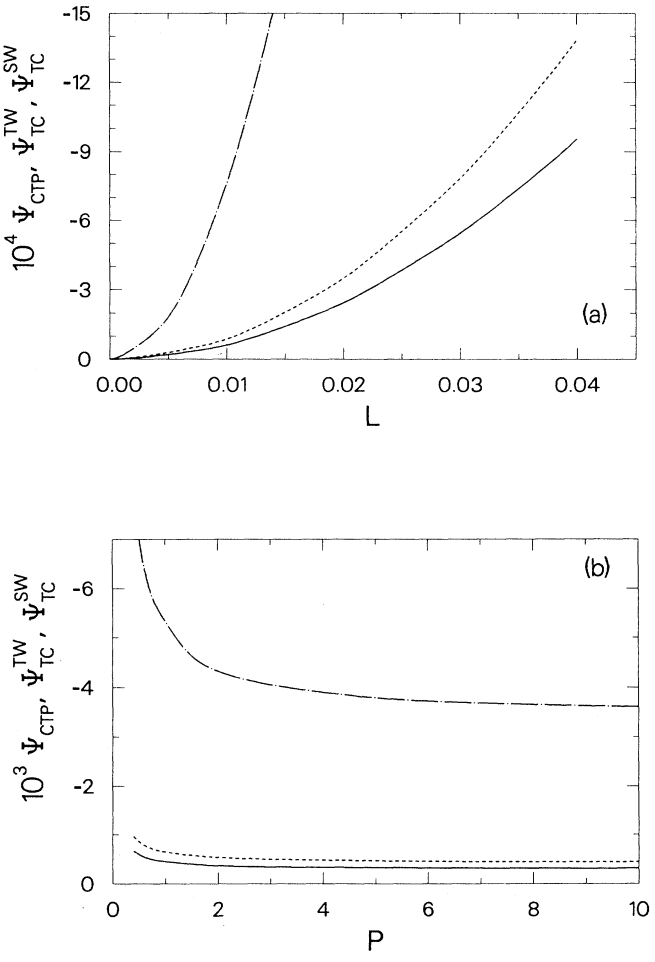

FIG. 9. Dependence of the codimension-2 point Ψ_{CTP} (solid lines), the tricritical point for traveling waves Ψ_{TC}^{TW} (dashed lines), and the tricritical point for standing waves Ψ_{TC}^{SW} (dot-dashed lines) on the material parameters: (a) as functions of L for fixed $P=0.6$ and (b) as functions of P for fixed $L=0.03$.

Our calculated value Ψ_{TC}^{TW} for the tricritical point of the TW's differ significantly (more than a factor of 10) from the experimentally measured one [13] and also from that obtained theoretically by a mode truncation analysis [22]. The value following from the mode truncation method is an approximation in itself, but additionally the wave number was adjusted to its value at $L=0$, which is not the optimal one [22]. A recent independent numerical calculation confirms our results [60]. The discrepancies with the experimental values for the tricritical point for TW's as well as for the SP (see below) may be due to several reasons. Near $\Psi=0$ the experimental determination of the actual value of the separation ratio Ψ is rather delicate for a ^{3}He-^{4}He mixture [61]. Furthermore, we have performed our calculation for an infinitely extended system while the experiments are of course always done in a finite container. For the tricritical point for the SP we always found $\Psi_{TC}^{stat}<0$, a fact that is in agreement with very classical theoretical results predicting the bifurcation to be supercritical at least for $\Psi=0$ [58]. This remains true if non-Boussinesq effects favoring rolls are included [23] and seems to be in conflict with some experiments in ^{3}He-^{4}He mixtures, where $\Psi_{TC}^{stat}>0$ was found [13]. It was shown for $\Psi=0$, however, that asymmetries caused, e.g., by a state equation similar to Eq. (2.2), but including in addition a quadratic expansion coefficient, may result in a backward bifurcation to hexagons [62]. This is a possible explanation for the discrepancy. Unfortunately the form of the convection pattern cannot be deduced from the experiments of Ref. [13].

Our perturbative determination of the weakly nonlinear behavior is in some sense complementary to full numerical calculations [26] and to an expansion around the limit of the normal fluid [27]. The latter one is restricted to the range $\Psi \ll -L^2$ and therefore excludes the interesting regime near the CTP. Also, with the full numerical calculations, the location of the points Ψ_{TC}^{TW}, Ψ_{CTP}, and Ψ_{TC}^{stat} are presumably not resolvable due to the limited accuracy of numerical methods. Our calculations are restricted to a small region around threshold, so that they are not applicable to fully developed nonlinear convection, where the other methods show their power. However, our results for the coefficients of Eqs. (1.1a) and (1.1b) allow us to make contact between different investigations of these amplitude equations and convection experiments in binary fluids. Examples are the measurements and calculations of Refs. [15] and [47] and the quantitative agreement between the direct measurement of the nonrescaleable coefficients of the amplitude equation [15] and our calculated values (see also Refs. [25,28]).

IV. CODIMENSION-2 BIFURCATION

The thresholds for the SP and for the Hopf bifurcation are equal for a slightly negative Ψ, so the very interesting case of a codimension-2 bifurcation arises (see Sec. III and Refs. [24,25]). Near such a point, rich dynamical behavior can be expected [48], which is one of the reasons why binary fluid convection has attracted great attention. The dynamics in the vicinity of a CTP can be described by a generalized amplitude equation, now second order in time, which was first derived in Ref. [38] for the case of free and permeable boundary conditions, where the critical wave numbers coincide at the CTP ($k_c^{osc}=k_c^{stat}$). For realistic boundary conditions, however, the critical wave numbers for the stationary and the oscillatory bifurcation are not identical at the CTP [24,25]. Therefore one expects in the weakly nonlinear range near the CTP new characteristics due to this wave-number difference [41].

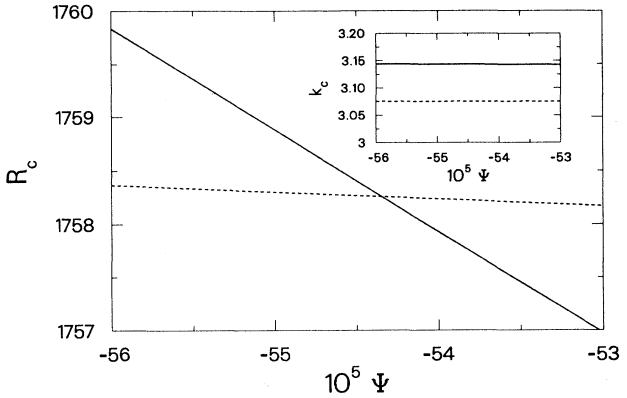

FIG. 10. Enlargement of the stability diagram of Fig. 1 near the codimension-2 point for $L=0.03$, $P=0.6$. The solid lines represent the stationary bifurcation, the dashed lines the Hopf bifurcation. The lines for the critical Rayleigh numbers intersect at $\Psi_{CTP}=-5.4346\times10^{-4}$. The inset shows the critical wave numbers, which are different here.

In this section all figures and numerical values correspond to a fluid with Lewis number $L=0.03$ and Prandtl number $P=0.6$. Figure 10 is an enlargement of Fig. 1 in the neighborhood of the CTP. The solid and dashed lines show the respective critical Rayleigh numbers R_c^{stat} and R_c^{osc}; in the inset we give the critical wave numbers k_c^{stat} and k_c^{osc}. In Fig. 11 the neutral curves $R_0(k)$ are given near the CTP for three different values of Ψ. Again, the solid lines correspond to the SP [$R_0^{stat}(k)$] and the dashed lines to the Hopf bifurcation [$R_0^{osc}(k)$]. In Fig. 11(a) we have $\Psi=\Psi_{CTP}=-5.4346\times10^{-4}$, in Fig. 11(b) $\Psi=-5.33\times10^{-4}>\Psi_{CTP}$, and in Fig. 11(c) $\Psi=-5.54\times10^{-4}<\Psi_{CTP}$. An important fact is that the neutral curve for the Hopf bifurcation (dashed line) ceases to exist when it reaches the neutral curve for the SP (solid line). Here the two (imaginary) eigenvalues degenerate to zero, and therefore also the frequency vanishes. Hence the Hopf frequency ω_c [i.e., the frequency at the minimum of the curve $R_0^{osc}(k)$] is nonzero at the CTP. From Fig. 11 one can also see that there is already an overlap of the two neutral curves for $\epsilon=(R-R_c^{osc})/R_c^{osc}<10^{-3}$. In this range the canonical amplitude equations given in Eqs. (1.1a) and (1.1b) are no longer applicable, because the assumption that all eigenmodes except the critical one are strongly damped is violated (see Sec. IV A). Therefore the more general CTP amplitude equation (1.2) has to be used here.

A. Degenerate CTP amplitude equation

Near the CTP two eigenvalues of the linear problem are near zero, so that the respective eigenmodes are only

weakly damped or weakly growing, whereas all the other eigenvalues are large and negative. Therefore in the vicinity of the CTP the linear dynamics can be described phenomenologically by a second-order characteristic polynomial,

$$\sigma^2-e(R,k)\sigma-d(R,k)=0\ . \tag{4.1}$$

With the arguments following Eq. (2.15) the conditions $e=0$ and $d=0$ give the neutral curves $R_0^{\rm osc}(k)$ and $R_0^{\rm stat}(k)$, respectively. Expansions of e and d up to leading orders yield

$$e=\beta R_c^{\rm osc}\left[\frac{R-R_c^{\rm osc}}{R_c^{\rm osc}}-\xi_{0,\rm osc}^2(k-k_c^{\rm osc})^2\right], \tag{4.2a}$$

$$d=\delta R_c^{\rm stat}\left[\frac{R-R_c^{\rm stat}}{R_c^{\rm stat}}[1+g_1\xi_{0,\rm stat}(k-k_c^{\rm stat})]-\xi_{0,\rm stat}^2(k-k_c^{\rm stat})^2-g_3\xi_{0,\rm stat}^3(k-k_c^{\rm stat})^3\right], \tag{4.2b}$$

with positive constants β and δ [41]. The generic normal form that reflects this linear and also the weakly nonlinear behavior of this codimension-2 type and incorporates the invariance under space-time translations and space reflections is given by Eq. (1.2) for appropriately scaled time and space coordinates. The terms with g_1, g_3, f_4, and f_5 have been kept in Eq. (1.2) to have consistently all terms up to the order $O(\eta^4)$. These terms have been neglected in Ref. [41] because they provide no essential contribution in the limit $\eta\to 0$, but we shall see below that they make corrections up to 5% in the present system. Strictly speaking, Eq. (1.2) describes a codimension-3 bifurcation with r, s, and η as control parameters. However, to apply, this equation to binary fluid convection, η is fixed by the small finite wavenumber difference at the CTP (see below). As one consequence, the interesting CTP features occur at finite values of r and s in Eq. (1.2), and not in the limit $r,s\to 0$.

For identifying the generic structure of Eq. (1.2), it is useful to keep only nonrescaleable parameters, as has been done in Ref. [41]. After this form is found, however, it is more useful to transform back to the physical coordinates to allow easier contact to the real system and in our context to the amplitude equations given in Sec. III. Equation (1.2) then reads

$$\partial_t^2 A-\beta R_c^{\rm osc}\left[\frac{R-R_c^{\rm osc}}{R_c^{\rm osc}}+\xi_{0,\rm osc}^2(\partial_x-ip)^2\right]\partial_t A+\frac{\delta}{\beta}[(f_2+f_3)|A|^2\partial_t A+f_3A^2\partial_t A^*]$$
$$-\delta R_c^{\rm stat}\left[\frac{R-R_c^{\rm stat}}{R_c^{\rm stat}}(1-ig_1\xi_{0,\rm stat}\partial_x)+\xi_{0,\rm stat}^2\partial_x^2-ig_3\xi_{0,\rm stat}^3\partial_x^3\right]A+f_1\frac{\delta^2}{\beta^2}|A|^2A$$
$$-i\frac{\delta^2}{\beta^2}\xi_{0,\rm stat}[f_4|A|^2\partial_x A+f_5A^2\partial_x A^*]=0\ . \tag{4.3}$$

The fast variation $e^{ik_c^{\rm stat}x}$ is separated out, so that with $A=Fe^{i(qx+\omega t)}$, the SP is now given by $q_c=0$ and the Hopf bifurcation by $q_c=p$. Equation (1.2) can be recovered from Eq. (4.3) by introducing the dimensionless parameters $r=(\beta^2/\eta^2\delta)(R-R_c^{\rm osc})$, $s=(\beta^2/\eta^2\delta)(R_c^{\rm osc}-R_c^{\rm stat})$ and $P_k=(p/\eta)[(\beta^2\xi_{0,\rm osc}^2R_c^{\rm osc})/\delta]^{1/2}$ with $p=k_c^{\rm osc}-k_c^{\rm stat}$. The time and space scaling is given by $t=(\beta/\eta\delta)T$ and $x=(1/\eta)[(\beta^2\xi_{0,\rm osc}^2R_c^{\rm osc})/\delta]^{1/2}X$, respectively, and the other values are $A=\eta\tilde{A}$, $a=\xi_{0,\rm stat}^2R_c^{\rm stat}/\xi_{0,\rm osc}^2R_c^{\rm osc}$, $g_1=\tilde{g}_1h$, $g_3=\tilde{g}_3(\xi_{0,\rm osc}^2R_c^{\rm osc}/\xi_{0,\rm stat}^2R_c^{\rm stat})h=\tilde{g}_3g_1/\tilde{g}_1a$, and $f_{4,5}=\tilde{f}_{4,5}h$ with $h=(\beta^2\xi_{0,\rm osc}^2R_c^{\rm osc}/\delta\xi_{0,\rm stat}^2)^{1/2}$. The coefficients of Eq. (4.3) are considered as independent of the Rayleigh number and the separation ratio and are determined in Sec. IV B below.

The simplest spatially periodic solutions of Eq. (4.3) are the SP

$$A=Fe^{iqx}\ \text{ with }\ F=\left[d(R,q)\frac{\beta^2}{\delta^2f_1}\right]^{1/2} \tag{4.4a}$$

and the TW's

$$A=Fe^{i(qx-\omega t)}\ \text{ with }\ F=\left[e(R,q)\frac{\beta}{\delta f_2}\right]^{1/2} \tag{4.4b}$$

and

$$\omega=\left[e(R,q)\frac{\delta}{\beta f_2}[f_1+\xi_{0,\rm stat}q(f_4-f_5)]-d(R,q)\right]^{1/2}.$$

In most of the known real systems showing a Hopf bifurcation, ω decreases with increasing control parameter R. This is the case only if $f_1+\xi_{0,\rm stat}q(f_4-f_5)<f_2$ [see Eq. (4.4b)]. It is expected by the general analysis and will turn out below that $\xi_{0,\rm stat}q(f_4-f_5)$ is only a small correction to f_1. Thus for decreasing $\omega(R)$ only two possibilities are left near the CTP: a forward bifurcation of the SP ($f_1>0$) and $f_1<f_2$ or a backward bifurcation of the SP ($f_1<0$). In binary fluid convection the SP in fact bifurcates backward at the CTP and ω decreases with increasing R, so this is consistent with the general arguments. On the curve of vanishing frequency $[\omega(R,\Psi)=0]$, the TW solution coincides with the SP solution.

The stability of these solutions against inhomogeneous perturbations $v(x,t)$ and also the relative stability of the simple SP, TW, and SW solutions have been investigated to some extent in Ref. [41] by discussing the characteristic fourth-order polynomial obtained from Eq. (4.3) after linearization with respect to the perturbations.

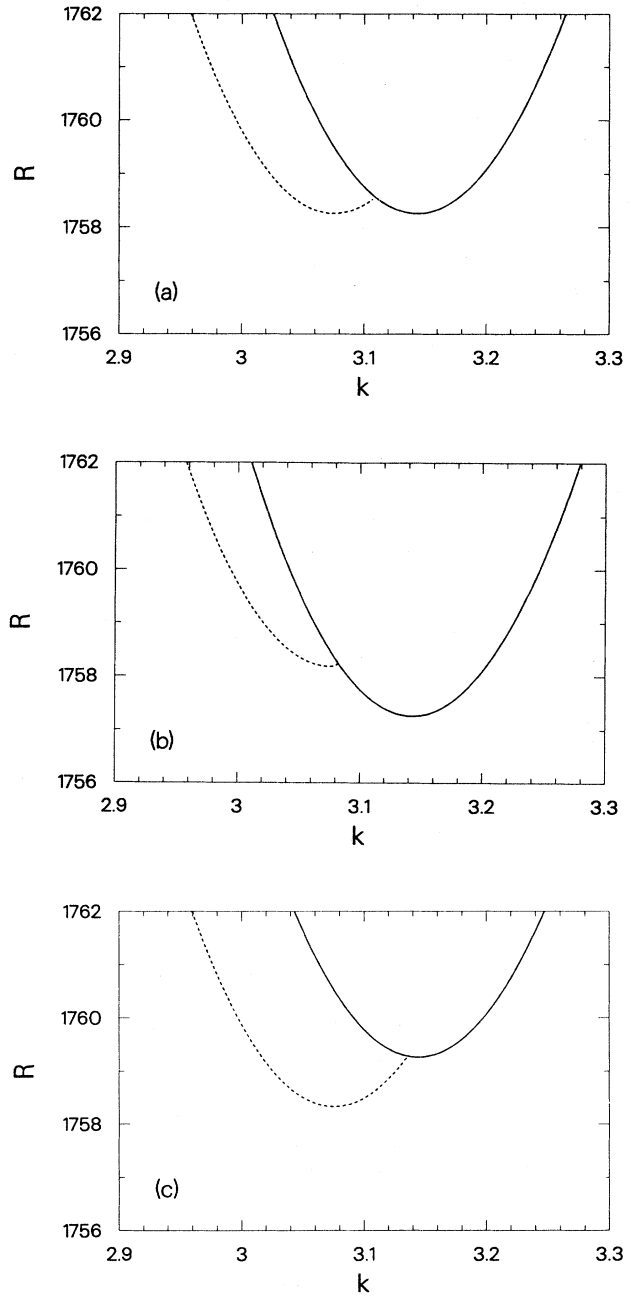

FIG. 11. Neutral curves for the stationary bifurcation (solid lines) and for the Hopf bifurcation (dashed lines) near the codimension-2 point for $L=0.03$ and $P=0.6$. (a) $\Psi=-5.4346\times10^{-4}=\Psi_{\rm CTP}$, (b) $\Psi=-5.33\times10^{-4}>\Psi_{\rm CTP}$, (c) $\Psi=-5.54\times10^{-4}<\Psi_{\rm CTP}$.

B. Canonical amplitude equations and coefficients of the CTP amplitude equation

In Ref. [41] it was shown that the main stability properties of each simple solution against sideband perturbations can be recovered by deriving from Eq. (4.3) the respective canonical amplitude equations (first-order in time) of the type of Eqs. (1.1a) and (1.1b) and calculating the stability with these simpler equations. The relative stability of these simple solutions can also be calculated by regarding coupled amplitude equations of similar forms. Moreover, the derivation of the canonical amplitude equations from Eq. (4.3) leads to relations between the coefficients of Eqs. (1.1a) and (1.1b) given in Sec. III and the still unknown coefficients of Eq. (4.3). From this we also get a measure for the range of validity of these equations near the CTP. Thus we derive in the following different canonical amplitude equations from Eq. (4.3).

1. Stationary bifurcation

In the limit $|R-R_c^{\rm stat}|/R_c^{\rm stat}\ll|R_c^{\rm osc}-R_c^{\rm stat}|/R_c^{\rm stat}$ it makes sense to look at the stationary solution of the linear part of Eq. (4.3), $A=e^{iqx}$ with $q_c=0$. An expansion of this solution around $R_c=R_c^{\rm stat}$, $q_c=0$ with the ansatz

$$A=\epsilon^{1/2}B(X,T)\quad\text{with}\quad\epsilon=\frac{R-R_c^{\rm stat}}{R_c^{\rm stat}} \tag{4.5}$$

and the time and space scaling $T=\epsilon t$, $X=\epsilon^{1/2}x$ leads after insertion into Eq. (4.3) to a solvability condition at order $\epsilon^{3/2}$, which represents the amplitude equation (3.2) for the stationary bifurcation

$$\frac{\beta R_c^{\rm osc}}{\delta R_c^{\rm stat}}\left[\xi_{0,\rm osc}^2(k_c^{\rm osc}-k_c^{\rm stat})^2-\frac{R_c^{\rm osc}-R_c^{\rm stat}}{R_c^{\rm stat}}\right]\partial_T B$$
$$=B+\xi_{0,\rm stat}^2\partial_X^2 B-f_1\frac{\delta}{\beta^2 R_c^{\rm stat}}|B|^2B\ . \tag{4.6}$$

By comparison we get expressions for $\tau_0^{\rm stat}$ and $\alpha^{\rm stat}$.

2. Hopf bifurcation

Here we look at the limit $|R-R_c^{\rm osc}|/R_c^{\rm osc}\ll|R_c^{\rm osc}-R_c^{\rm stat}|/R_c^{\rm stat}$ for a linear solution of Eq. (4.3) of the form $A=e^{i(\omega t+qx)}$ with $q_c=p$ and $\omega=\omega_c$ (see below). Again we make an expansion around $R_c=R_c^{\rm osc}$, $q_c=p$ with the ansatz

$$A=\epsilon^{1/2}[C_1(X,T,T_1)e^{i\omega_c t}+C_2(X,T,T_1)e^{-i\omega_c t}]e^{iq_c x}$$
$$\text{with}\quad\epsilon=\frac{R-R_c^{\rm osc}}{R_c^{\rm osc}}\ . \tag{4.7}$$

We have introduced the two times $T=\epsilon t$ and $T_1=\epsilon^{1/2}t$ and for the space scaling $X=\epsilon^{1/2}x$. Inserting this into Eq. (4.3) leads at order ϵ to an expression for the group velocity v_g and at order $\epsilon^{3/2}$ to the coupled amplitude equations for the Hopf bifurcation, Eqs. (1.1a) and (1.1b).

3. *Coefficients of the CTP amplitude equation and consistency relations*

Now comparing Eq. (4.6) with Eq. (3.2) and the coupled equations following from the expansion (4.7) with Eq. (1.1a) and (1.1b), we obtain the following general expressions for the linear values ($p=k_c^{\rm osc}-k_c^{\rm stat}$):

$$\tau_0^{\rm stat}=\frac{\beta R_c^{\rm osc}}{\delta R_c^{\rm stat}}\left[\xi_{0,\rm osc}^2 p^2-\frac{R_c^{\rm stat}-R_c^{\rm osc}}{R_c^{\rm osc}}\right], \tag{4.8a}$$

$$\omega_c^2=\delta R_c^{\rm stat}\left[\xi_{0,\rm stat}^2 p^2(1+g_3\xi_{0,\rm stat}p)-\frac{R_c^{\rm osc}-R_c^{\rm stat}}{R_c^{\rm stat}}(1+g_1\xi_{0,\rm stat}p)\right], \tag{4.8b}$$

$$v_g=\frac{\delta R_c^{\rm stat}}{\omega_c}\xi_{0,\rm stat}\left[\xi_{0,\rm stat}p(1+\tfrac{3}{2}g_3\xi_{0,\rm stat}p)-\frac{g_1}{2}\frac{R_c^{\rm osc}-R_c^{\rm stat}}{R_c^{\rm stat}}\right], \tag{4.8c}$$

$$\tau_0^{\rm osc}=\frac{2}{\beta R_c^{\rm osc}}, \tag{4.8d}$$

$$c_0=-\frac{\delta}{\beta\omega_c}(1+g_1\xi_{0,\rm stat}p), \tag{4.8e}$$

$$c_1=\frac{\delta R_c^{\rm stat}\xi_{0,\rm stat}^2}{\beta R_c^{\rm osc}\xi_{0,\rm osc}^2\omega_c}\left[\frac{v_g^2}{\delta R_c^{\rm stat}\xi_{0,\rm stat}^2}-1-3g_3\xi_{0,\rm stat}p\right], \tag{4.8f}$$

and for the nonlinear coefficients

$$\alpha^{\rm stat}=\frac{\delta}{\beta^2 R_c^{\rm stat}}f_1, \tag{4.9a}$$

$$\alpha^{\rm osc}=\frac{\delta}{\beta^2 R_c^{\rm osc}f_2}, \tag{4.9b}$$

$$c_2=-\frac{\delta^2}{\beta^3 R_c^{\rm osc}\omega_c}[f_1+\xi_{0,\rm stat}p(f_4-f_5)], \tag{4.9c}$$

$$\gamma=\frac{2\delta}{\beta^2 R_c^{\rm osc}}f_3, \tag{4.9d}$$

$$c_3=-\frac{2\delta^2}{\beta^3 R_c^{\rm osc}\omega_c}[f_1+\xi_{0,\rm stat}p(f_4-f_5)]=2c_2. \tag{4.9e}$$

With these relations, together with the numerical values given in Tables I and II, we are able to calculate the new coefficients except one of Eq. (4.3). Due to the fact that we have more equations than unknown quantities, some connections between the coefficients of the amplitude equation for the stationary bifurcation and those for the Hopf bifurcation have to be fulfilled at the CTP. As we have described in Sec. II, these amplitude equations (3.2) and (3.3) have been obtained by independent perturbation expansions starting from the basic equations. Therefore such consistency relations allow further checks for our numerical calculations of Sec. III.

For the linear values we have the six relations (4.8a)–(4.8f) for the four unknown coefficients β, δ, g_1, and g_3, so due to this multiplicity two consistency checks are left. The general expressions of Eqs. (4.8a)–(4.8f) become simpler when being calculated at the CTP, where $R_c^{\rm osc}=R_c^{\rm stat}=R_{\rm CTP}$. From Eqs. (4.8a) and (4.8d) we get β and δ, and from Eqs. (4.8b) and (4.8e) we get g_1 and g_3 (the coefficients g_1 and g_3 describing the asymmetry of the neutral curve are given for the case of a simple fluid with free boundaries in Ref. [36]). With these values we first see that the correction due to g_1 in Eq. (4.8e) is about 5% and the corrections due to g_3 are 3% in Eq. (4.8b) and 4.5% in Eq. (4.8c). If we now calculate v_g according to Eq. (4.8c), we get $v_g=-0.665$ instead of the numerical value -0.661 given in Table II, which is a discrepancy of about 0.6%. The value of $c_1=0.194$ from Eq. (4.8f) seems to deviate too much from 0.26 (see Table II), but here we have to keep in mind that c_1 varies strongly near the CTP (see Fig. 5) and that without the g_3 correction Eq. (4.8f) would give $c_1=0$. So the CTP amplitude equation (4.3) forces a behavior of c_1, which is unexpected from earlier work [25,28], but was found by our improved numerics discussed in Sec. III.

The five equations (4.9a)–(4.9e) for the nonlinear values yield the four coefficients f_1, f_2, f_3, and (f_4-f_5), so one consistency check is left, namely, $c_3=2c_2$ [see Eq. (4.9e)], which is fulfilled to about 5%. With the equations discussed we cannot derive f_4 and f_5 independently. The correction due to (f_4-f_5) is about 1.6%. In Table III we give all the coefficients of Eq. (4.3) for $L=0.03$ and $P=0.6$ at the CTP.

4. *Zero group velocity near the codimension-2 point*

From the calculation of the threshold behavior we know that the group velocity v_g is positive over most of the Ψ range [see also Ref. [25]]. However, it changes sign at $\Psi\approx-1.25\times10^{-3}$ and is negative at the CTP. This is consistent with the general behavior following from Eq. (4.3) [see Eq. (4.8c) and the discussion in the preceding paragraph]. From Eq. (4.8c), we can calculate the zero of the analytical expression valid for v_g near the CTP, yielding

TABLE III. Coefficients of the codimension-2 amplitude equation (4.3) for $L=0.03$, $P=0.6$ at $\Psi_{\rm CTP}=-5.4346\times10^{-4}$.

$R_{\rm CTP}=1758.26$	$\beta=0.00612$	$f_1=-291.04$
$p=-0.0681$	$\delta=0.0018$	$f_2=4.94$
$\xi_{0,\rm osc}^2=0.152$	$g_1\xi_{0,\rm stat}p=-0.051$	$f_3=339.37$
$\xi_{0,\rm stat}^2=0.149$	$g_3\xi_{0,\rm stat}p=-0.0304$	$(f_4-f_5)\xi_{0,\rm stat}p=4.536$

$$\frac{R_c^{\rm osc}-R_c^{\rm stat}}{R_c^{\rm stat}}=-\frac{2}{g_1}\xi_{0,\rm stat}(k_c^{\rm stat}-k_c^{\rm osc})\times[1-\tfrac{3}{2}g_3\xi_{0,\rm stat}(k_c^{\rm stat}-k_c^{\rm osc})]\ . \quad (4.10)$$

Inserting the values of Table III and translating the threshold difference into the separation ratio, we get $\Psi(v_g=0)\approx -1.06\times10^{-3}$. This is somewhat larger than that calculated directly in Sec. III, but still in reasonable agreement (note that on the Ψ scale this point is already about one order of magnitude away from the CTP, we had $\Psi_{\rm CTP}=-5.4346\times10^{-4}$). This result gives us an estimate for the validity range of Eq. (4.3), i.e., down to which value of $\Psi<\Psi_{\rm CTP}$ the second time derivative of Eq. (4.3) is relevant. Obviously the tricritical point for TW's, $\Psi_{\rm TC}^{\rm TW}=-7.850\times10^{-4}$, is also included. An amplitude equation describing this tricritical point and that for the SP, in addition to the CTP, is given in Appendix A.

The zero of v_g is a general feature of the CTP equation (4.3), as can be seen from Eq. (4.8c). To occur, however, inside the range of existence for the Hopf bifurcation, the inequality $p/g_1<0$ has to hold, which is in fact the case for binary fluid convection.

5. *Interaction between traveling waves and stationary pattern*

In the limit

$$\frac{|R-R_c^{\rm osc}|}{R_c^{\rm osc}},\frac{|R-R_c^{\rm stat}|}{R_c^{\rm stat}},\frac{|R_c^{\rm stat}-R_c^{\rm osc}|}{R_c^{\rm stat}}\ll\xi_{0,\rm stat}^2p^2\ ,$$

when the difference between the thresholds of the SP and of the TW is small compared to the wave-number difference, the interaction between the two TW solutions and the SP can be investigated in terms of three coupled canonical amplitude equations, which are derivable from Eq. (4.3). For this purpose we now expand simultaneously around the linear solutions of Eq. (4.3) for the SP, $A^{\rm stat}=e^{iqx}$ with $q_c^{\rm stat}=0$ and for the TW, $A^{\rm osc}=e^{i(\omega t+qx)}$ with $q_c^{\rm osc}=p$ and $\omega=\omega_c$. For simplicity we only study the interaction of one TW solution with the SP, so we formally make the ansatz

$$A=\epsilon_0^{1/2}B(T_0,T_1,X_0)e^{i(\omega_c t+px)}+\epsilon_s^{1/2}D(T_s,X_s)\ , \quad (4.11a)$$

with

$$\epsilon_0=\frac{R-R_c^{\rm osc}}{R_c^{\rm osc}}\ \text{ and }\ \epsilon_s=\frac{R-R_c^{\rm stat}}{R_c^{\rm stat}}\ , \quad (4.11b)$$

with the different time and space scaling $T_0=\epsilon_0 t$, $T_1=\epsilon_0^{1/2}t$, $T_s=\epsilon_s t$ and $X_0=\epsilon_0^{1/2}x$, $X_s=\epsilon_s^{1/2}x$, but with ϵ_0 and ϵ_s of the same order. So we get at order $\epsilon_{0,s}^{3/2}$ solvability conditions in the form of coupled equations for B and D, which read, after rescaling back to the physical units,

$$\tau_0^{\rm stat}\partial_t D=\epsilon_s D+\xi_{0,\rm stat}^2\partial_x^2 D-\alpha^{\rm stat}|D|^2D-(\gamma_2+ic_4)|B|^2D\ , \quad (4.12a)$$

$$\tau_0^{\rm osc}(\partial_t-v_g\partial_x)B=\epsilon_0(1+ic_0)B+\xi_{0,\rm osc}^2(1+ic_1)\partial_x^2B-(\alpha^{\rm osc}+ic_2)|B|^2B-(\gamma_3+ic_5)|D|^2B\ . \quad (4.12b)$$

The coefficients $\tau_0^{\rm stat}$, $\tau_0^{\rm osc}$, v_g, c_0, c_1, $\alpha^{\rm stat}$, $\alpha^{\rm osc}$, and c_2 are given in Eqs. (4.8a)–(4.8f) and (4.9a)–(4.9e), and the new coupling coefficients are

$$\gamma_2=\frac{\delta}{\beta^2R_c^{\rm stat}}[2f_1+\xi_{0,\rm stat}p(f_4-2f_5)]\ , \quad (4.13a)$$

$$c_4=\frac{\omega_c}{\beta R_c^{\rm stat}}(f_2-f_3)\ , \quad (4.13b)$$

$$\gamma_3=\frac{\delta}{\beta^2R_c^{\rm osc}}(f_2+f_3)\ , \quad (4.13c)$$

$$c_5=-\frac{\delta^2}{\beta^3R_c^{\rm osc}\omega_c}(2f_1+\xi_{0,\rm stat}pf_4)\ . \quad (4.13d)$$

If we had derived Eqs. (4.12a) and (4.12b) directly from the basic equations as was done in Sec. II for Eqs. (1.1a) and (1.1b), the coefficients $\gamma_{2,3}$ and $c_{4,5}$ would be known. So we could in principle calculate f_4 and f_5 independently and three more consistency checks would be left.

C. Traveling-wave stability near the CTP

In Ref. [41] it was predicted on a phenomenological level that the supercritically bifurcating TW's become Benjamin-Feir unstable in some neighborhood of the CTP. It was shown that this phenomenon is induced only by the characteristics at the CTP: supercritically bifurcating TW's, subcritically bifurcating SP, and finite wave-number difference, which is all fulfilled in binary fluid convection (see Sec. III). Since the coefficients of Eq. (4.3) have been determined, we can now repeat quantitatively the arguments of Ref. [41] and we can compare with the direct calculation of the Benjamin-Feir instability described in Sec. III.

The criterion for Benjamin-Feir instability of the TW solution (4.4b) calculated in the framework of the full CTP equation (4.3) is equivalent with [31,39,41]

$$\frac{c_1c_2}{\alpha^{\rm TW}}<-1\ , \quad (4.14)$$

with c_1,c_2 given by Eqs. (4.8f) and (4.9c) and $\alpha^{\rm TW}$ is $\alpha^{\rm osc}$ of Eq. (4.9b). Using the equality in Eq. (4.14) to get the boundaries of the unstable interval, we can rewrite this into a second-order polynomial for $\bar{s}=(R_c^{\rm osc}-R_c^{\rm stat})/R_c^{\rm stat}$. It turns out that one solution, $\bar{s}_{\rm min}$, is negative and $O(1)$, while the other one can be expanded in powers of $\xi_{0,\rm stat}p$, leading to

$$\bar{s}_{\rm max}=g_3\xi_{0,\rm stat}^3p^3+O(\xi_{0,\rm stat}^4p^4)\ . \quad (4.15)$$

With the values of Table III we obtain $\bar{s}_{\rm max}=-2.1\times10^{-5}$ which corresponds after translating into the separation ratio to $\Psi=-5.4388\times10^{-4}$. For Ψ below this value the TW's are Benjamin-Feir unstable and this value agrees very well with that obtained directly

in Sec. III. On the other hand, it was shown in Sec. III that the boundary for Benjamin-Feir instability is essentially given by the zero of c_1, due to the steepness of c_1 near this point. If we calculate this zero from Eq. (4.8f), we get in lowest order of $\xi_{0,\mathrm{stat}}p$ the same expansion as given in Eq. (4.15), so this is also consistent with our numerical result. Via the analysis described here it becomes clear now that the origin of the Benjamin-Feir stable range for the TW's is induced by the finite wave-number difference $k_c^{\mathrm{osc}}-k_c^{\mathrm{stat}}$.

To investigate the question up to which value of the reduced Rayleigh number $\epsilon_0=(R-R_c^{\mathrm{osc}})/R_c^{\mathrm{osc}}$ the TW solution exists stably inside the interval $[\bar{s}_{\max},\bar{s}=0]$, one has to remember that the frequency ω_c decreases near the CTP with increasing ϵ [see Eq. (4.4b)]. Neglecting the small correction terms g_1 and g_3, we find from Eq. (4.4b) together with Eqs. (4.2a) and (4.2b) and $q=p$ the curve where the frequency vanishes:

$$\epsilon_{\mathrm{H}}=\left[-\bar{s}+\frac{R_c^{\mathrm{stat}}}{R_c^{\mathrm{osc}}}\xi_{0,\mathrm{stat}}^2p^2\right]\frac{f_2}{f_2-f_1}\ . \tag{4.16}$$

Near the CTP, the relative distance $\bar{s}$ of the two thresholds is proportional to $(\Psi-\Psi_{\mathrm{CTP}})$. Due to the finite Hopf frequency at the CTP, ϵ_H is finite, too, and from Table III we find $\epsilon_H^{\mathrm{CTP}}=1.15\times10^{-5}$. The slope of the curve (4.16) inside the ϵ-$\bar{s}$ plane is given by $\partial\epsilon_H/\partial s=f_2/(f_1-f_2)=-0.0167$. As indicated in Ref. [41], however, the TW's become unstable against sideband perturbations already before reaching the curve $\omega(R,\Psi)=0$. This is due to the finite wave-number difference between the SP and the Hopf bifurcation near the CTP. The instability of the TW can in principle be calculated from Eq. (4.3), but more simply by taking first the limits leading to Eqs. (4.12a) and (4.12b). Investigating then the stability of the equilibrium TW solution $|B|=\epsilon_0/\alpha^{\mathrm{osc}}$ of Eq. (4.12a) at the band center, we find that small perturbations $|D|\ll(\epsilon_s/\alpha^{\mathrm{state}})^{1/2}$ grow for $\epsilon_0>\epsilon_{\mathrm{sp}}:=\bar{s}f_2/(f_2-2f_1)$. At the CTP we have $\epsilon_{\mathrm{sp}}=0$ and because of $f_2\ll|f_1|$ the slope of ϵ_{sp} with $\bar{s}$ has roughly half the value as the slope of ϵ_{H}, more definitely $\partial\epsilon_{\mathrm{sp}}/\partial\bar{s}=f_2/(2f_1-f_2)=-0.0084$.

So the TW's become unstable against a stationary roll pattern for very small $\epsilon\sim10^{-5}$ and the range of stable TW's near the CTP seems to be unmeasurably small for fluid mixtures. Perhaps gas mixtures would allow the investigation of the discussed effects.

D. Discussion and outlook

By extracting from the degenerate amplitude equation (4.3) valid near the CTP the limits of the SP and the Hopf bifurcation, we have determined all the coefficients except one of this new equation from the already known ones of Eqs. (1.1a) and (1.1b). In this way we found very helpful consistency relations and could identify some special features of the TW's as intrinsic CTP properties. So the sign change of the group velocity v_g and the Benjamin-Feir instability can be interpreted as typical CTP phenomena. Also, a minimal range of validity for the CTP equation (4.3), at least with respect to its linear properties is given by the point $\Psi(v_g=0)$.

For small values of L one finds $(k_c^{\mathrm{osc}}-k_c^{\mathrm{stat}})=:p\propto L$ and $\omega_c\propto L$ at the CTP (see also Ref. [25]), Ψ_{CTP}, $\Psi_{\mathrm{TC}}^{\mathrm{TW}}$, and $\Psi_{\mathrm{TC}}^{\mathrm{SW}}\propto L^2$ and $\Psi_{\mathrm{TC}}^{\mathrm{stat}}\propto L^3$, an observation which has various consequences for the ranges of validity of the different analytical descriptions in the vicinity of the CTP. When using the canonical amplitude equations (1.1a) and (1.1b), the dynamics of the amplitudes A and B have to be slow on the scale of the inverse Hopf frequency $1/\omega_c$, which imposes near the CTP the restriction $\epsilon,|A|^2\ll\omega_c\propto L$. Also, the overlap region of the neutral curves shown in Figs. 11(a)–11(c), and therefore the parameter range where $\omega(R,\Psi)=0$, must be avoided. Due to this, the even stronger restriction $\epsilon,|A|^2\ll p^2\propto L^2$ must be respected when using Eqs. (1.1a) and (1.1b) near the CTP. To cover also the overlap region of the neutral curves, the more general equation (4.3) may be used in the larger range $(R-R_c)/R_c\approx p^2\propto L^2$, which represents a circle with radius $O(L^2)$ around the crossover of the two threshold curves of Fig. 10. This region, however, also includes the tricritical points $\Psi_{\mathrm{TC}}^{\mathrm{TW}}$ and $\Psi_{\mathrm{TC}}^{\mathrm{stat}}$, and then the validity of Eq. (4.3) over the full regime becomes questionable, because near a tricritical point, fifth-order terms have to be included [44–46]. To include both the tricritical behavior and the full dynamics of the CTP, an extension of Eq. (1.2) up to quintic order in the amplitude must be done. This is briefly sketched in Appendix A, where the new equation is derived by symmetry arguments (see also [29,41,40]). This rather complicated equation (A1) should then cover situations where $p\propto L$ and $|\Psi_{\mathrm{TC}}^{\mathrm{TW,stat}}-\Psi_{\mathrm{CTP}}|\propto L^2$, and is valid for $(R-R_c)/R_c\propto L^2$.

One assumption for the derivation of the amplitude equations is the fact that all modes of the linear part of the Eqs. (2.5b)–(2.5d), except the critical one given by Eq. (2.16), are damped on a sufficiently short time scale so that they can be adiabatically eliminated. In our case an x-independent solution $\mathbf{u}_{\mathrm{hom}}=(0,\eta_{\mathrm{hom}}(z,t),0)$ of the linear part of Eqs. (2.5b)–(2.5d) exists and has a damping rate L, so its typical time scale is $1/L$. Comparing away from the CTP the time scale $1/\epsilon$ for the mode $Ae^{i(k_cx+\omega_ct)}$ and $1/L$ for $\mathbf{u}_{\mathrm{hom}}$, we can now distinguish three regimes for increasing ϵ ($\epsilon\ll1$): $\epsilon\ll L^2$ (regime I), $\epsilon=O(L^2)$ (regime II), and $\epsilon=O(L)$ (regime III). Obviously, in regime I the dynamics of $\mathbf{u}_{\mathrm{hom}}$ are much faster than those of mode A and can thus be adiabatically eliminated. This regime mainly gives the range of validity for our canonical amplitude equations.

In the limit of large Prandtl numbers the mode $\mathbf{u}_{\mathrm{hom}}(z)=(0,f(z),0)$ is antisymmetric with respect to the middle of the fluid layer ($z=\frac{1}{2}$) and for free boundary conditions one has explicitly $\mathbf{u}_{\mathrm{hom}}(z)=(0,\sin(2\pi z),0)$ [63]. Choosing $\epsilon=O(L)$ and adding now $C\mathbf{u}_{\mathrm{hom}}(z)$ to the ansatz (2.16), one can derive the coupled amplitude equations

$$\begin{aligned}\tau_0(\partial_t-(v_g+v_CC)\partial_x)A=[&\epsilon(1+ic_0)+\xi_0^2(1+ic_1)\partial_x^2\\&+d_1C+d_2C^2+d_3\partial_xC\\&-(\alpha+ic_2)|A|]A\ ,\end{aligned} \tag{4.17a}$$

$$\tau_C \partial_t C = (a_L + b_1 \partial_x^2 + b_2 |A|) C + e_1 |A| + e_2 \partial_x |A| + e_3 A \partial_x A^* \ . \tag{4.17b}$$

Again, both amplitudes A and C vary slowly on the scales of the wavelength $2\pi/k_c$ and of the inverse Hopf frequency $2\pi/\omega_c$ of the pattern. The structure of these equations has been described for free and permeable boundary conditions in Refs. [63], where the terms d_2, d_3, and v_C were omitted. The additional terms b_i and v_C for the Hopf bifurcation are usually complex, while τ_C, d_i, e_i are real and $a_L \propto L$ are real constants. By construction, Eqs. (4.17a) and (4.17b) hold in regime III. In regime II the scaling $\epsilon \propto L^2$ leads to a similar set of equations, now with vanishing coupling coefficients $b_1 = b_2 = e_2 = e_3 = 0$.

To include the behavior near a tricritical point, an extension of the canonical amplitude equations up to quintic order, as discussed above, would be sufficient in regime I. When proceeding near the tricritical point to regime II, one violates the above-described restrictions $\epsilon, |A|^2 \ll L^2$ for the canonical amplitude equations. Therefore the homogeneous mode couples to the generalized equation given in Appendix A, and not to a canonical amplitude equation up to quintic order. So the coupling of $\mathbf{u}_{\text{hom}}(t)$ to one of the amplitude equations (1.1a) or (1.1b) seems relevant only in the strongly subcritical range of the TW, where calculations on the dispersive chaos [15] were done with an amplitude equation up to cubic order [43,47]. Still existing quantitative differences between theory [43,47] and experiment [15] may originate from the fact that the calculations are done in regime I, while the experiments mostly correspond to regime II or III.

V. INFLUENCE OF THERMAL NOISE

A. Modified basic equations

In principle thermal noise is always present in convection experiments, but is negligible in most situations. Nevertheless, noise may actually trigger the convection above onset, which without any disturbances would not be manifested. Near the convection onset the system is most sensitive to thermal fluctuations and their influence have been directly detected in two recent experiments [18,55]. To consider a stochastic influence theoretically, the basic equations (2.1b)–(2.1d) have to be generalized by including the respective fluctuating terms. In the case of thermal noise in simple fluid convection, these terms have been given by Landau and Lifshitz [56] for the velocity and the temperature fluctuations. We have in addition calculated the term describing the concentration fluctuations along the lines of their derivation [64] (see also Ref. [65]). With the dimensionless scaling from Sec. II A we again get the equations for the deviations from the heat conduction state (2.5a)–(2.5d), now with the following additional terms on their rhs's (for a more detailed discussion see Ref. [52]; summation over doubly occurring indices is assumed):

$$-\nabla\cdot\mathbf{q} \ , \quad -\nabla\cdot\mathbf{i} \ , \quad -\partial_z(\partial_j s_{xj}) + \partial_x(\partial_j s_{zj}) \ . \tag{5.1}$$

Here $\mathbf{q}$, $\mathbf{i}$, and s_{ij} are stochastic terms with the autocorrelation functions

$$\langle q_i(\mathbf{r},t) q_j(\mathbf{r}',t') \rangle = 2Q_1 \delta_{ij} \delta(\mathbf{r}-\mathbf{r}') \delta(t-t') \ , \tag{5.2a}$$

$$\langle s_{ij}(\mathbf{r},t) s_{lm}(\mathbf{r}',t') \rangle = 2Q_2 (\delta_{il}\delta_{jm} + \delta_{im}\delta_{jl}) \times \delta(\mathbf{r}-\mathbf{r}') \delta(t-t') \ , \tag{5.2b}$$

$$\langle i_i(\mathbf{r},t) i_j(\mathbf{r}',t') \rangle = 2Q_3 \delta_{ij} \delta(\mathbf{r}-\mathbf{r}') \delta(t-t') \ , \tag{5.2c}$$

and no cross correlations. The Q_i are the strengths of the respective thermal fluctuations [64,65]:

$$Q_1 = k_B T_0^2 \frac{g^2 \alpha^2 d^3}{\nu^2 \kappa^2 \rho_0 c_p} \ , \quad Q_2 = k_B T_0 \frac{\nu}{d \kappa^3 \rho_0} \ ,$$
$$Q_3 = k_B T_0 \frac{D}{\frac{\partial \mu}{\partial c} \Psi^2} \frac{g^2 \beta^2 d^3}{\nu^2 \kappa^3 \rho_0} \ . \tag{5.3}$$

The new parameters are the Boltzmann constant k_B, the heat capacity c_p, and the chemical potential μ. c is the concentration in the original scaling, so $\partial\mu/\partial c$ is a parameter in original units. T_0 is the absolute working temperature.

Due to the Soret effect and the Dufour effect one would in principle also have fluctuating terms with nonvanishing cross correlations. These have been neglected for simplicity, and it will turn out later that the main contribution comes from the velocity fluctuations given by Q_2, while the other contributions are at least three orders of magnitude smaller.

B. Amplitude expansion

Following Graham [52,66], one can derive an amplitude equation similar to Eq. (3.3) with an additional term describing the noise. We have generalized this derivation to the case of binary fluids and we here briefly outline the differences to Grahams's results. Our Eq. (2.18) now becomes

$$(\mathcal{M}\partial_t + \mathcal{L})\mathbf{u} = \mathbf{N}(\mathbf{u},\mathbf{u}) + \mathbf{I} \ , \tag{5.4}$$

with $\mathbf{I}$ being the vector of the new terms (5.1). We again insert the expansion $\mathbf{u} = \epsilon^{1/2}\mathbf{u}_0 + \epsilon\mathbf{u}_1 + \epsilon^{3/2}\mathbf{u}_2$ with $\epsilon = (R - R_c)/R_c$ and formally also the slow variables $X = \epsilon^{1/2}x$ and $T = \epsilon t$. In the stochastic terms the fast variation is separated out (variations in the y direction are again omitted, due to the quasi-one-dimensional situation under consideration):

$$q_i(x,z,t) = \hat{q}_i(X,z,T) e^{i(k_c x + \omega_c t)} + \text{c.c.} \ , \tag{5.5a}$$

$$i_i(x,z,t) = \hat{i}_i(X,z,T) e^{i(k_c x + \omega_c t)} + \text{c.c.} \ , \tag{5.5b}$$

$$s_{ij}(x,z,t) = \hat{s}_{ij}(X,z,T) e^{i(k_c x + \omega_c t)} + \text{c.c.} \ , \tag{5.5c}$$

with $\langle \hat{q}_i \hat{q}_j \rangle = \langle \hat{i}_i, \hat{i}_j \rangle = \langle \hat{s}_{ij}, \hat{s}_{lm} \rangle = 0$. Here the terms with $\hat{q}_i$, $\hat{i}_i$, and $\hat{s}_{ij}$ describe the noise at positive wave numbers and frequencies only [66], so that the resulting correlations are

$$\langle \hat{q}_i^*(X,z,T)\hat{q}_j(X',z',T')\rangle = 2Q_1\delta_{ij}\delta(X-X')\delta(z-z')\delta(T-T') , \tag{5.6a}$$

$$\langle \hat{s}_{ij}^*(X,z,T)\hat{s}_{lm}(X',z',T')\rangle = 2Q_2(\delta_{il}\delta_{jm}+\delta_{im}\delta_{jl})\delta(X-X')\delta(z-z')\delta(T-T') , \tag{5.6b}$$

$$\langle \hat{i}_i^*(X,z,T)\hat{i}_j(X',z',T')\rangle = 2Q_3\delta_{ij}\delta(X-X')\delta(z-z')\delta(T-T') . \tag{5.6c}$$

These fluctuating terms are considered small. Therefore, with the same arguments as in Ref. [52], **I** contributes only at highest order $\epsilon^{3/2}$ (if $Q_1,Q_2,Q_3<\epsilon^{3/2}$). Since the linear coefficients except Q of Eq. (1.3) are already known from Sec. III, we need to consider only the fast variables x and t for the actual amplitude expansion. This is analogous to Sec. II C 3 in order to get the simplified derivation of the amplitude equation. So we again end up with Eqs. (2.26a) and (2.26b), while Eq. (2.26c) is replaced by

$$(\mathcal{M}\partial_t+\mathcal{L}_0)\mathbf{u}_2=\mathbf{N}_2(\mathbf{u}_0,\mathbf{u}_1)-\mathcal{L}_2\mathbf{u}_0+\mathbf{I} \quad (\epsilon^{3/2}) . \tag{5.7}$$

Up to this order one has

$$\mathbf{I}=e^{i(k_c x+\omega_c t)}\begin{bmatrix} -ik_c\hat{q}_x-\partial_z\hat{q}_z \\ -ik_c\hat{i}_x-\partial_z\hat{i}_z \\ -ik_c\partial_z\hat{s}_{xx}-\partial_z^2\hat{s}_{xz}-k_c^2\hat{s}_{zx}+ik_c\partial_x\hat{s}_{zz}\end{bmatrix} + \text{c.c.} \tag{5.8}$$

With the ansatz

$$\mathbf{u}_2(x,z,t)=A_2\begin{bmatrix}\vartheta_2(z)\\ \eta_2(z)\\ \dfrac{1}{ik_c}\Phi_2(z)\end{bmatrix}e^{i(k_c x+\omega_c t)} ,$$

the projection of Eq. (5.7) on $\hat{\mathbf{u}}_0^\dagger$ yields a solvability condition similar to Eq. (2.27):

$$0=(1+ic_0)A_0+(1+ic_0)\frac{I_2}{I_1}|A_0|^2A_0 + \frac{1+ic_0}{I_1}\int_0^1\hat{\mathbf{u}}_0^{\dagger *}(z)\hat{\mathbf{I}}(z)dz , \tag{5.9}$$

where I_1 and I_2 are defined in Eq. (2.27) and

$$\hat{\mathbf{I}}(z)=\begin{bmatrix} -ik_c\hat{q}_x-\partial_z\hat{q}_z \\ -ik_c\hat{i}_x-\partial_z\hat{i}_z \\ -k_c^2\partial_z\hat{s}_{xx}+ik_c\partial_z^2\hat{s}_{xz}+ik_c^3\hat{s}_{zx}+k_c^2\partial_z\hat{s}_{zz}\end{bmatrix} . \tag{5.10}$$

Defining now $\sqrt{Q}F:=[(1+ic_0)/I_1]\int_0^1\hat{\mathbf{u}}_0^{\dagger *}\cdot\hat{\mathbf{I}}\,dz$, we recover Eq. (1.3) from Eq. (5.9) after considering again the slow variables. The integral $\int_0^1\hat{\mathbf{u}}_0^{\dagger *}\cdot\mathbf{I}dz$ can be evaluated by integrating by parts. Following again Graham's calculation [52,66], we eventually get for the noise term in Eq. (1.3)

$$Q=2\left[\frac{1+ic_0}{I_1}\right]^2\left[Q_1\int_0^1[\partial_z\vartheta_0^{\dagger *}\partial_z\vartheta_0^\dagger+k_c^2\vartheta_0^{\dagger *}\vartheta_0^\dagger]dz+Q_2\int_0^1[k_c^2\partial_z^2\Phi_0^{\dagger *}\partial_z^2\Phi_0^\dagger-2k_c^4\Phi_0^{\dagger *}\partial_z^2\Phi_0^\dagger+k_c^6\Phi_0^{\dagger *}\Phi_0^\dagger]dz + Q_3\int_0^1[\partial_z\eta_0^{\dagger *}\partial_z\eta_0^\dagger+k_c^2\eta_0^{\dagger *}\eta_0^\dagger]dz\right] , \tag{5.11a}$$

with the correlation

$$\langle F^*(x,t)F(x',t')\rangle=\delta(x-x')\delta(t-t') \tag{5.11b}$$

and

$$\langle F(x,t)F(x',t')\rangle=0 .$$

This result is quite general and yields the strength of the noise term for realistic (rigid and impervious) as well as for unrealistic (free and pervious) boundary conditions for the stationary and for the Hopf bifurcation by evaluating Eq. (5.11a) with the respective eigenfunctions. This will be done in the following subsection.

C. Strength of the noise term

1. *Free, pervious boundary conditions*

For unrealistic boundaries, analytic linear solutions are known [9,38], and Q according to Eq. (5.11a) can in principle be calculated analytically. For the stationary bifurcation the relevant linear solutions are $\Phi_0(z)=\sqrt{2}\sin\pi z$, $\vartheta_0^\dagger(z)=(P/3)(1+\Psi)\sin\pi z$, $\eta_0^\dagger(z)=(P\Psi/3L)\sin\pi z$, $\Phi_0^\dagger(z)=\sin\pi z$, which yield for I_1 from Eq. (2.27) $I_1=(9\sqrt{2}/8)\pi^4P$. Inserting these expressions into Eq. (5.11a) eventually gives the noise term for the stationary bifurcation [with $k_c^2=\pi^2/2$, $R_c=\frac{27}{4}\pi^4a$, $a=1/(1+\Psi+\Psi/L)$]:

$$Q=\frac{4Pa}{9\pi^2}\left[Q_1\frac{(1+\Psi)^2}{R_cP}+Q_2\frac{1}{P^3a}+Q_3\frac{\Psi^2}{L^2R_cP}\right] . \quad (5.12)$$

With typical parameters one gets for a water-alcohol mixture $Q_1/(R_cP)\approx 7\times 10^{-16}$, $Q_2/P^3\approx 5\times 10^{-10}$, and $Q_3\Psi^2/(L^2R_cP)\approx 3\times 10^{-13}$ and for ^{3}He-^{4}He $Q_1/(R_cP)\approx 2\times 10^{-11}$, $Q_2/P^3\approx 6.3\times 10^{-7}$, and $Q_3\Psi^2/(L^2R_cP)\approx 9\times 10^{-10}$ (we have chosen $\Psi=0$). In both cases the most relevant contribution comes from the term with Q_2 and we can write

$$Q\approx\frac{4}{9\pi^2P^2}Q_2$$

$$\text{with } Q_2\approx\begin{cases}5\times 10^{-7} & \text{(water-alcohol)} \quad (5.13a)\\ 1.4\times 10^{-7} & (^3\text{He-}^4\text{He}) . \quad (5.13b)\end{cases}$$

Q does not depend on Ψ. Taking into account the different scaling, our result coincides with that derived previously by Graham for the case of a simple fluid ($\Psi=0$) [52], when a factor of 2 is included [66]. The noise term was also derived by a different method [53,54]. After accounting there for a factor of $\frac{1}{3}$ [67] one has agreement with the above result.

For the Hopf bifurcation the linear solutions are also known analytically, but due to the complexity of the involved integrals we give the numerical results. Q becomes complex here, but for the correlation function (see below) only $|Q|$ is important. Again, the largest contribution comes from the term with Q_2. For $L=0.01$, $P=10$ (water-alcohol) we obtain

$$Q\approx\begin{cases}(2.2+7.9i)\times 10^{-4}Q_2 & \text{for } \Psi=-0.5 \quad (5.14a)\\ (4.4+1.4i)\times 10^{-4}Q_2 & \text{for } \Psi=-0.05 , \quad (5.14b)\end{cases}$$

and for $L=0.03$, $P=0.6$ (^{3}He-^{4}He)

$$Q\approx\begin{cases}(15+3.2i)\times 10^{-2}Q_2 & \text{for } \Psi=-0.5 \quad (5.15a)\\ (11-3.7i)\times 10^{-2}Q_2 & \text{for } \Psi=-0.05 . \quad (5.15b)\end{cases}$$

$|Q|$ depends weakly on Ψ and is similar to the value for the stationary case.

2. Rigid, impervious boundary conditions

Here the integrals in Eq. (5.11a) have to be evaluated numerically and we give only the results. Again, it is sufficient to consider the term with Q_2. In the stationary case we find for $L=0.01$, $P=10$

$$Q\approx\begin{cases}2.3\times 10^{-4}Q_2 & \text{for } \Psi=0 \quad (5.16a)\\ 2.2\times 10^{-7}Q_2 & \text{for } \Psi=0.04 , \quad (5.16b)\end{cases}$$

and for $L=0.03$, $P=0.6$

$$Q\approx\begin{cases}6.5\times 10^{-2}Q_2 & \text{for } \Psi=0 \quad (5.17a)\\ 1.6\times 10^{-4}Q_2 & \text{for } \Psi=0.13 . \quad (5.17b)\end{cases}$$

Besides $\Psi=0$ we have chosen a value near Ψ_∞. We remind the reader that for positive Ψ there are qualitative differences between realistic and unrealistic boundaries also with respect to other quantities (e.g., the behavior of the critical wave number k_c, the coherence length ξ_0^2, or the relaxation time τ_0). The strong variation of Q with Ψ may be due to the same origin that leads to the divergence of the critical wavelength at $\Psi=\Psi_\infty$.

For the Hopf bifurcation we have for $L=0.01$, $P=10$

$$Q\approx\begin{cases}(2.7-3.6i)\times 10^{-4}Q_2 & \text{for } \Psi=-0.5 \quad (5.18a)\\ (1.9+1.5i)\times 10^{-4}Q_2 & \text{for } \Psi=-0.05 , \quad (5.18b)\end{cases}$$

and for $L=0.03$, $P=0.6$

$$Q\approx\begin{cases}(9.3-0.44i)\times 10^{-2}Q_2 & \text{for } \Psi=-0.5 \quad (5.19a)\\ (-2.4+5.9i)\times 10^{-2}Q_2 & \text{for } \Psi=-0.05 . \quad (5.19b)\end{cases}$$

Here the values are of the same order as for free, pervious boundary conditions.

D. Noise-induced amplitude

1. Correlation functions

Although one cannot solve Eq. (1.3) for the amplitude $A(x,t)$, it is nevertheless possible to discuss the space-time correlation function defined as

$$f_{\text{corr}}(A,\Delta x,\Delta t):=\langle A^*(x,t)A(x+\Delta x,t+\Delta t)\rangle=\frac{1}{(2\pi)^2}\int_{-\infty}^{+\infty}\int_{-\infty}^{+\infty}A^*(x,t)A(x+\Delta x,t+\Delta t)dx\,dt . \quad (5.20)$$

For the case of a simple fluid ($\Psi=0$), this has been done in detail in Ref. [52], starting from the full Eq. (1.3). In the subcritical regime ($\epsilon<0$), where one expects very small noise-induced amplitudes, it seems reasonable to neglect in a first approximation the nonlinear term in Eq. (1.3). In this case the correlation function (5.20) can be written down analytically (see Appendix B and Sec. V E; for the case $c_1=0$ see Refs. [18,55]). One gets for the zero-lag amplitude correlation ($\Delta x=\Delta t=0$)

$$f_{\text{corr}}(A,0,0):=\hat{A}^2=\frac{|Q|}{4\tau_0\xi_0\sqrt{-\epsilon}} . \quad (5.21)$$

This function would diverge at threshold ($\epsilon=0$) like $1/\sqrt{-\epsilon}$, but here one has to remember that the above amplitude expansion is valid only for $\epsilon\leq -10^{-6}$. Moreover, with increasing A the nonlinearities become important.

To get the correlation functions of the physical quantities, one has to start from the full linear solution (2.16). Within the approximation leading to the amplitude equation (1.3), i.e., the assumption that the amplitude $A(x,t)$ varies on a much slower scale than the critical mode $e^{i(k_cx+\omega_ct)}$, we have

$$f_{\mathrm{corr}}(f,\Delta x,\Delta t)=2|f_{\mathrm{corr}}(A,\Delta x,\Delta t)| \times|f(z)|^2\cos(k_c\Delta x+\omega_c\Delta t)\ , \tag{5.22}$$

with f being one of the functions ϑ, η, or Φ.

2. Relevant experimental quantities

In a thermal convection experiment the temperature variation is probably the quantity most easily measurable. For comparison of the measured temperature correlation function with our result (5.22) one has to insert ϑ for f and then scale back to the original units (see Sec. II). This yields for the zero-lag temperature correlation

$$\hat{T}^2:=f_{\mathrm{corr}}(T,0,0)=\frac{\Delta T^2}{R^2}|\vartheta_m|^2\,2\frac{|Q|}{4\tau_0\xi_0\sqrt{-\epsilon}}\ , \tag{5.23}$$

where $\vartheta_m=\vartheta_0(z=z_m)$ with ϑ_0 being the linear solution of Eq. (2.9) and z_m the position where the temperature variation is measured.

So the relevant quantities are not given only by the noise strength $|Q|$, but through the complete expressions (5.23). Inserting for $|Q|$ the respective parts of Eq. (5.11a), this yields together with Q_2 from Eq. (5.3) and the Rayleigh number R from (2.8)

$$\hat{T}^2\sqrt{-\epsilon}=\frac{k_BT_0\nu^3}{\beta_T^2g^2d^7\kappa\rho_0}\frac{|\vartheta_m|^2|\mathcal{F}|}{2\tau_0\xi_0} =:\frac{k_BT_0\nu^3}{\beta_T^2g^2d^7\kappa\rho_0}\mathcal{Q}_T(\Psi)\ . \tag{5.24}$$

Here $\mathcal{F}$ is the important part of Q from Eq. (5.11a), but without Q_2. Q_2 has been drawn into the prefactor, which consists of pure material parameters. $\mathcal{Q}_T$ is defined by Eq. (5.24) and depends on Ψ through ϑ_m, $\mathcal{F}$, τ_0, and ξ_0. For typical material parameters, one gets in the experimentally best realizable case ($\epsilon\approx-10^{-4}$) $\hat{T}\approx9\times10^{-5}$ K for water-alcohol and $\hat{T}\approx2\times10^{-6}$ K for ^{3}He-^{4}He, which both should be inside the measurable range (these values are for $\Psi=-0.2$). Analogous calculations yield for the concentration variation $\hat{N}\le10^{-7}$ and for the velocity variation $\hat{u}_z\le0.1$ $\mu m/$s, which both seem to be unmeasurably small.

In Fig. 12 we have plotted $\mathcal{Q}_T$ as a function of Ψ at $z=\frac{1}{2}$ for the special water-alcohol mixture used in Ref. [18] ($L=0.009$, $P=15.5$). In the case of the stationary bifurcation, this value varies strongly, therefore in Fig. 12(a) we show $\ln\mathcal{Q}_T$. For $\Psi=0$ one has $\mathcal{Q}_T\approx38$ and $\mathcal{Q}_T$ decreases over several orders of magnitude with increasing Ψ until Ψ_∞ is reached. This variation is mostly induced by τ_0, which becomes zero near the codimension-2 point and diverges for $\Psi=\Psi_\infty$ [see Fig. 2(b)]. As a consequence the influence of thermal fluctuations is amplified by the divergence inside the interval $[\Psi_{\mathrm{CTP}},0]$. For $\Psi<\Psi_{\mathrm{CTP}}$ the Hopf bifurcation has to be considered. Not too near to the codimension-2 point $\mathcal{Q}_T$ shows a much weaker dependence on Ψ [see Fig. 12(b)] and is of the same order as for the stationary bifurcation at $\Psi=0$. The values given here for realistic boundaries are in general twice as large as for free, impermeable boundary conditions.

For the Hopf bifurcation, $\mathcal{Q}_T$ increases strongly near the CTP. This fact has similar reasons as the increase of quantities such as, e.g., c_0 or c_2 here, and is probably induced by the competition between the stationary and the oscillatory bifurcation. More details of this amplification of thermal fluctuations near the CTP will be discussed elsewhere.

E. Discussion

In this section we have addressed the question of thermal noise influencing the bifurcation and have therefore derived the respective amplitude equations (1.3) for the Hopf bifurcation and the SP, now generalized by introducing a stochastic term. The only relevant contribution to this term comes from the velocity fluctuations, while the other fluctuating forces are at least three orders of magnitude smaller for realistic fluid parameters. For the Hopf bifurcation, the noise strength does not vary much with the separation ratio (except for the vicinity of the CTP); however, for the SP it decreases over several orders of magnitude with increasing Ψ.

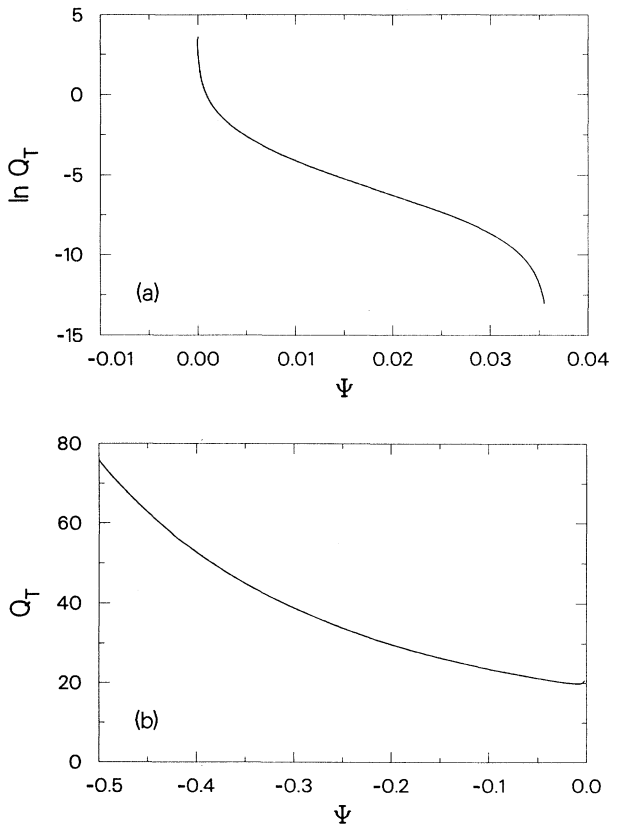

FIG. 12. $\mathcal{Q}_T$ from Eq. (5.24), which is the relevant quantity for the noise-induced temperature variation $\hat{T}^2$ for $L=0.009$, $P=15.5$. (a) $\ln\mathcal{Q}_T$ for the stationary bifurcation. (b) $\mathcal{Q}_T$ for the Hopf bifurcation.

In Appendix B we have derived an analytical expression for the space-time correlation function of the amplitude by neglecting the nonlinear term in Eq. (1.3) which is valid in the subcritical regime ($\epsilon<0$). To discuss the result, we rewrite Eq. (B11) in a slightly different form by introducing the intensity $\hat{A}^2=|Q|/(4\tau_0\xi_0\sqrt{\bar{\epsilon}})$, the length $x_0=\xi_0/(\bar{\epsilon})^{1/2}$, and the times $t_0=\tau_0/\bar{\epsilon}$ and $t_1=\xi_0/(v_g\sqrt{\bar{\epsilon}})$ ($\bar{\epsilon}=-\epsilon$, $\bar{c}_1=1+ic_1$):

$$f_{\rm corr}(A,\Delta x,\Delta t)=\tfrac{1}{2}\hat{A}^2 e^{ic_i\Delta t/t_0}\left\{\exp\left[-\left[\frac{\Delta x}{x_0}+\frac{\Delta t}{t_1}\right]\right]\operatorname{erfc}\left\{\left[\bar{c}_1\frac{\Delta t}{t_0}\right]^{1/2}-\frac{1}{2\sqrt{\bar{c}_1}}\left[\frac{\Delta x/x_0}{(\Delta t/t_0)^{1/2}}+\left[\frac{t_0\Delta t}{t_1^2}\right]^{1/2}\right]\right\}\right.$$
$$\left.+\exp\left[+\left[\frac{\Delta x}{x_0}+\frac{\Delta t}{t_1}\right]\right]\operatorname{erfc}\left\{\left[\bar{c}_1\frac{\Delta t}{t_0}\right]^{1/2}+\frac{1}{2\sqrt{\bar{c}_1}}\left[\frac{\Delta x/x_0}{(\Delta t/t_0)^{1/2}}+\left[\frac{t_0\Delta t}{t_1^2}\right]^{1/2}\right]\right\}\right\}. \quad (5.25)$$

This correlation function shows some very interesting features. First of all one gets a nonexponential decay when including spatial degrees of freedom, even in the case of a stationary bifurcation where $c_1=v_g=0$. This is in contrast to Ref. [52], where an exponential decay was predicted [66] by mistake. A naive single-mode model [Eq. (B1) without spatial derivatives] would give the correlation function $f_{\rm corr}(A,\Delta t)=(|Q|/2\tau_0\bar{\epsilon})e^{-\Delta t/t_0}$. Here one has an exponential decay and moreover the intensity goes like $1/\bar{\epsilon}$ rather than $1/\sqrt{\bar{\epsilon}}$ in Eq. (5.25). It has been shown, however, that this is not compatible with measurements, whereas Eq. (5.25) fits the experimental data quite well [18,55].

Another striking property is that two correlation times t_0 and t_1 occur naturally. t_0 measures the decay of a spatially periodic state $Ae^{i(kx+\omega t)}$ with $A=$const, while t_1 corresponds to the spatial decay of a modulated state passing the observer with the group velocity v_g. Due to the different scaling laws, these two times can be extracted from the experimental data independently. Because of the linear approximation of Eq. (B1), these correlation times together with the correlation length x_0 and the intensity $\hat{A}^2$ diverge at the bifurcation point ($\bar{\epsilon}=0$), a behavior that is quite analogous to phase transitions in equilibrium thermodynamics. These divergences are of course not real, but a strong increase of the respective values near $\epsilon=0$ is still present even with saturating nonlinear terms.

In a recent experiment on binary fluid convection [18], good agreement with the theoretical values of the correlation times yielding different orders of magnitude for t_0 and t_1 and especially the correct scaling laws were found. The noise strength was compared with the analog of Eq. (5.24) for free, pervious boundary conditions. As we mentioned in Sec. V D, however, this strength does not change drastically for realistic boundaries and within the experimental uncertainties the agreement holds for realistic boundaries, also.

ACKNOWLEDGMENTS

We thank Pierre Hohenberg, Robert Graham, Eberhard Bodenschatz, Peter Lucas, and especially Ingo Rehberg and Lorenz Kramer for many hints and discussions.

APPENDIX A: AMPLITUDE EQUATION COVERING THE CTP AND THE TRICRITICAL POINTS

Our numerical results and some scaling considerations given in Sec. IV have shown that the tricritical points for the TW's as well as for the SP still lie inside the validity range of at least the linear part of the CTP amplitude equation (4.3). As a consequence this equation cannot be applied to the full range including these points, where different scaling laws have to be taken into account. In a small vicinity of the tricritical points of the order $|\Psi_{\rm TC}^{\rm TW}-\Psi_{\rm CTP}|$, an amplitude equation including also fifth-order terms may cover the full nonlinear behavior. Such equations describing the transition regime from supercritical to subcritical behavior are well known and considerably investigated away from the CTP (see [44–46] and references therein). To include now the tricritical points into the generalized CTP amplitude equation (4.3), we extend the calculations presented in the Appendix of Ref. [29], where spatial derivatives and the wave-number difference between the stationary and the Hopf bifurcation have been omitted.

The generic normal form, which reflects the linear behavior of the CTP neighborhood, and which incorporates the invariance under space-time translation and space reflection, and which moreover includes the tricritical points of the TW's and of the SP, is then given by

$$\partial_T^2\overline{A}-\eta[r+(\partial_X-iP_k)^2]\partial_T\overline{A}+(\eta\bar{f}_2+f_3)|\overline{A}|^2\partial_T\overline{A}+f_3\overline{A}^2\partial_T\overline{A}^*+\eta f_6|\overline{A}|^4\partial_T\overline{A}+\eta f_7|\overline{A}|^2\overline{A}^2\partial_T\overline{A}^*+\eta f_8|\partial_T\overline{A}|^2\overline{A}$$
$$-i\eta(f_9|\overline{A}|^2\partial_T+f_{10}\overline{A}^*\partial_T\overline{A}+f_{11}\overline{A}\partial_T\overline{A}^*)(\partial_X-iP_k)\overline{A}-i\eta(f_{12}\overline{A}\partial_T\overline{A}+f_{13}\overline{A}^2\partial_T)(\partial_X+iP_k)\overline{A}^*$$
$$-[(r+s)(1-i\eta\tilde{g}_1\partial_X)+a\partial_X^2-i\eta\tilde{g}_3\partial_X^3-\bar{f}_1|\overline{A}|^2-f_{14}|\overline{A}|^4-\eta f_{15}|\overline{A}|^6]\overline{A}$$
$$-i(\tilde{f}_4|\overline{A}|^2\partial_X\overline{A}+\tilde{f}_5\overline{A}^2\partial_X\overline{A}^*+\eta f_{16}|\overline{A}|^4\partial_X\overline{A}+\eta f_{17}|\overline{A}|^2\overline{A}^2\partial_X\overline{A}^*)=0\ . \quad (A1)$$

Here the fast variation e^{ikx} (with $k=k_c^{\text{stat}}$ at the CTP) is separated out. The amplitude of the physical quantities $A \propto \sqrt{\eta}\,\bar{A}$ and the coefficients $f_{1,2}$ are assumed to be small near the tricritical points for the TW's and for the SP. Therefore we have introduced the new coefficients $\bar{f}_{1,2}$ with $f_{1,2}=\eta \bar{f}_{1,2}$. Space and time coordinates as well as the control parameter η and the wave number difference P_k are scaled as in Sec. IV. The term f_{15} must be included to have the terms at order η completely.

APPENDIX B: SPACE-TIME CORRELATION OF THE NOISE-INDUCED AMPLITUDE

We want to derive an analytical expression for the correlation function (5.20) of the convection amplitude in the subcritical regime starting from Eq. (1.3). Here $\epsilon<0$ and for the expected very small amplitudes it is possible to neglect the nonlinear terms. The coefficient c_0 is transformed away by a time-dependent phase factor and for further convenience we set $\bar{\epsilon}=-\epsilon>0$. So we regard the linear equation

$$\tau_0(\partial_t - v_g\partial_x)A = -\bar{\epsilon}A + \xi_0^2(1+ic_1)\partial_x^2 A + \sqrt{Q}F(x,t) , \tag{B1}$$

with the complex prefactor Q of the noise term and the space-time correlation

$$\begin{aligned} &\langle F^*(x,t)F(x+\Delta x,t+\Delta t)\rangle = \delta(\Delta x)\delta(\Delta t) , \\ &\langle F(x,t)F(x+\Delta X,t+\Delta t)\rangle = 0 . \end{aligned} \tag{B2}$$

Using Fourier techniques we can calculate the space-time correlation function

$$\begin{aligned} f_{\text{corr}}(A,\Delta x,\Delta t) &:= \langle A^*(x,t)A(x+\Delta x,t+\Delta t)\rangle \\ &= \frac{1}{(2\pi)^2}\int_{-\infty}^{+\infty}\int_{-\infty}^{+\infty} A^*(x,t)A(x+\Delta x,t+\Delta t)dx\,dt . \end{aligned} \tag{B3}$$

For this purpose we introduce the pair of Fourier transforms in space and time

$$g(x,t)=\int_{-\infty}^{+\infty}\int_{-\infty}^{+\infty}\bar{g}(k,\omega)e^{i(kx+\omega t)}dk\,d\omega , \tag{B4a}$$

$$\bar{g}(k,\omega)=\frac{1}{(2\pi)^2}\int_{-\infty}^{+\infty}\int_{-\infty}^{+\infty} g(x,t)e^{-i(kx+\omega t)}dx\,dt , \tag{B4b}$$

where the overbar denotes the Fourier transform of the respective function. The Fourier transform of the correlation function (with respect to Δx and Δt) is simply given by the product of the Fourier transforms of the single functions:

$$\begin{aligned} \overline{f_{\text{corr}}(A,\Delta x,\Delta t)} &= \overline{\langle A^*(x,t)A(x+\Delta x,t+\Delta t)\rangle} \\ &= \bar{A}^*(k,\omega)\bar{A}(k,\omega) , \end{aligned} \tag{B5}$$

so we first get from Eq. (B2)

$$\langle F^*(x,t)F(x+\Delta x,t+\Delta t)\rangle = \bar{F}^*(k,\omega)\bar{F}(k,\omega)=\frac{1}{(2\pi)^2} . \tag{B6}$$

Now inserting the Fourier transforms (B4a) into Eq. (B1) yields

$$\bar{A}(k,\omega)=\frac{\sqrt{Q}\bar{F}(k,\omega)}{[\bar{\epsilon}+\xi_0^2k^2(1+ic_1)]+i(\omega-v_gk)\tau_0} , \tag{B7}$$

so we have

$$\bar{A}^*(k,\omega)\bar{A}(k,\omega) = \frac{|Q|}{(2\pi)^2}\frac{1}{(\bar{\epsilon}+\xi_0^2k^2)^2+[\xi_0^2k^2c_1+(\omega-v_gk)\tau_0]^2} . \tag{B8}$$

Now we can transform back into the physical space

$$f_{\text{corr}}(A,\Delta x,\Delta t) = \int_{-\infty}^{+\infty}\int_{-\infty}^{+\infty}\bar{A}^*(k,\omega)\bar{A}(k,\omega)e^{ik\Delta x}e^{i\omega\Delta t}dk\,d\omega , \tag{B9}$$

which gives after some substitutions for ω

$$f_{\text{corr}}(A,\Delta x,\Delta t)=\frac{|Q|}{(2\pi)^2\tau_0}\int_{-\infty}^{+\infty}e^{ik(\Delta x+v_g\Delta t)}e^{-i(c_1/\tau_0)\xi_0^2k^2\Delta t}\left[\int_{-\infty}^{+\infty}\frac{e^{i(\omega/\tau_0)\Delta t}}{(\bar{\epsilon}+\xi_0^2k^2)^2+\omega^2}d\omega\right]dk . \tag{B10}$$

The second integral can be evaluated by help of the residium theorem yielding $[\pi/(\bar{\epsilon}+\xi_0^2k^2)]\exp[-(\bar{\epsilon}+\xi_0^2k^2)(\Delta t/\tau_0)]$. So we get from Eq. (B10)

$$f_{\rm corr}(A,\Delta x,\Delta t)=\frac{|Q|}{4\pi\tau_0\xi_0^2}e^{-(\bar\epsilon/\tau_0)\Delta t}\int_{-\infty}^{+\infty}\frac{e^{ik(\Delta x+v_g\Delta t)}}{k^2+(\bar\epsilon/\xi_0^2)}e^{-(1+ic_1)\xi_0^2k^2(\Delta t/\tau_0)}dk$$

$$=\frac{|Q|}{2\pi\tau_0\xi_0^2}e^{-(\bar\epsilon/\tau_0)\Delta t}\int_{0}^{+\infty}\frac{\cos[k(\Delta x+v_g\Delta t)]}{k^2+(\bar\epsilon/\xi_0^2)}e^{-(1+ic_1)\xi_0^2k^2(\Delta t/\tau_0)}dk$$

$$=\frac{|Q|}{8\tau_0\xi_0\sqrt{\bar\epsilon}}e^{i\bar\epsilon c_1(\Delta t/\tau_0)}\left\{e^{-(\bar\epsilon/\epsilon_0^2)^{1/2}(\Delta x+v_g\Delta t)}\operatorname{erfc}\left[[\bar\epsilon\bar c_1(\Delta t/\tau_0)]^{1/2}-\frac{\Delta x+v_g\Delta t}{2[\bar c_1\xi_0^2(\Delta t/\tau_0)]^{1/2}}\right]\right.$$

$$\left.+e^{+(\bar\epsilon/\epsilon_0^2)^{1/2}(\Delta x+v_g\Delta t)}\operatorname{erfc}\left[\left[\bar\epsilon\bar c_1\frac{\Delta t}{\tau_0}\right]^{1/2}+\frac{\Delta x+v_g\Delta t}{2[c_1\xi_0^2(\Delta t/\tau_0)]^{1/2}}\right]\right\} \tag{B11}$$

[see e.g., Ref. [68]; here $\operatorname{erfc}(x)=1-\operatorname{erf}(x)$, where $\operatorname{erf}(x)$ is the usual error function]. We have set $\bar c_1=1+ic_1$. The result for $c_1=0$ ($\bar c_1=1$) and Q real has been given in Refs. [18,55].

The zero-lag correlation follows by evaluating the integrals in Eq. (B10) with $\Delta t=\Delta x=0$ leading to the result of Eq. (5.21),

$$f_{\rm corr}(A,0,0)=\langle|A(x,t)|^2\rangle=\frac{|Q|}{4\tau_0\xi_0\sqrt{\bar\epsilon}}\ . \tag{B12}$$

[1] (a) *Hydrodynamical Instabilities and the Transition to Turbulence,* edited by H. L. Swinney and J. P. Gollub (Springer, New York, 1981); (b) *Propagation in Systems Far from Equilibrium,* edited by J. E. Wesfreid, H. R. Brand, P. Manneville, G. Albinet, and N. Boccara Springer Series in Synergetics Vol. 41 (Springer, New York, 1988); (c) *New Trends in Nonlinear Dynamics and Pattern-Forming Phenomena: The Geometry of Nonequilibrium,* edited by P. Coullet and P. Huerre (Plenum, New York, 1990); (d) *Nonlinear Evolution of Spatio-Temporal Structures in Dissipative Continuous Systems,* edited by F. H. Busse and L. Kramer (Plenum, New York, 1990); (e) *Nonlinear Science: The Next Decade,* edited by D. Campbell, R. Ecke, and J. M. Hyman [special issue in Physica D **51** (1991)].

[2] H. Bénard, Rev. Gen. Sci. Pures Appl. **11**, 1261 (1900); **11**, 1309 (1900); Lord Rayleigh, Philos. Mag. **32**, 529 (1916).

[3] For an overview see, e.g., S. Chandrasekhar, *Hydrodynamic and Hydromagnetic Stability* (Oxford University Press, London, 1961).

[4] F. H. Busse, in *Hydronamical Instabilities and the Transition to Turbulence* (Ref. [1(a)]), p. 97; Prog. Theor. Phys. **41**, 1929 (1978).

[5] For an overview see, e.g., E. Dubois-Violette, G. Durand, E. Guyon, P. Manneville, and P. Pieranski, in *Solid State Physics,* Suppl. 14, edited by L. Liebert (Academic, New York, 1987); P. J. Barratt, Liq. Cryst. **4**, 223 (1989).

[6] G. I. Taylor, Philos. Trans. R. Soc. **223**, 289 (1923); for an overview see R. C. di Prima and Harry L. Swinney, in *Hydronamical Instabilities and the Transition to Turbulence* (Ref. [1a]), p. 139.

[7] For a recent overview see, e.g., W. Zimmermann, Mater. Res. Bull. **16**, 46 (1991); for more specialized viewpoints see I. Rehberg, B. L. Winkler, M. de la Torre Juárez, S. Rasenat, and W. Schöpf, Feskörperprobleme **29**, 35 (1989); S. Kai and W. Zimmermann, Prog. Theor. Phys. **99**, 458 (1989).

[8] See, e.g., G. Z. Gershuni and E. M. Zhukhovitskii, *Convective Stability of Incompressible Fluids* (Keter, Jerusalem, 1976).

[9] For a review of the older literature see, e.g., J. K. Platten and L. C. Legros, *Convection in Liquids* (Springer, New York, 1984).

[10] E. Knobloch, Phys. Rev. A **34**, 1538 (1986).

[11] G. W. T. Lee, P. Lucas, and A. Tyler, J. Fluid Mech. **135**, 235 (1983).

[12] I. Rehberg and G. Ahlers, Phys. Rev. Lett. **55**, 500 (1985).

[13] G. Ahlers and I. Rehberg, Phys. Rev. Lett. **56**, 1372 (1986); T. S. Sullivan and G. Ahlers, *ibid.* **61**, 78 (1988).

[14] R. W. Walden, P. Kolodner, A. Passner, and C. M. Surko, Phys. Rev. Lett. **55**, 496 (1985); C. M. Surko and P. Kolodner, *ibid.* **61**, 842 (1988); P. Kolodner, D. Bensimon, and C. M. Surko, *ibid.* **60**, 1723 (1988).

[15] P. Kolodner, J. A. Glazier, and H. Williams, Phys. Rev. Lett. **65**, 1579 (1990); J. A. Glazier, P. Kolodner, and H. Williams, J. Stat. Phys. **64**, 945 (1991).

[16] E. Moses and V. Steinberg, Phys. Rev. A **34**, 693 (1986); Phys. Rev. Lett. **60**, 2030 (1988); J. Fineberg, E. Moses, and V. Steinberg, *ibid.* **61**, 838 (1988).

[17] O. Lhost and J. K. Platten, Phys. Rev. A **38**, 3147 (1988); **40**, 6415 (1989).

[18] W. Schöpf and I. Rehberg, Europhys. Lett. **17**, 321 (1992).

[19] J. C. Legros, D. Longree, G. Chavepeyer, and J. K. Platten, Physica A **80**, 76 (1975); D. P. Chock and Chin-Hsiu Li, Phys. Fluids **18**, 1401 (1975).

[20] H. R. Brand and V. Steinberg, Phys. Lett. **93A**, 333 (1983); Physica A **119**, 327 (1983).

[21] S. J. Linz and M. Lücke, Phys. Rev. A **35**, 3997 (1987); G. Ahlers and M. Lücke, *ibid.* **35**, 470 (1987).

[22] S. J. Linz, M. Lücke, H. W. Müller, and J. Niederländer, Phys. Rev. A **38**, 5727 (1988).

[23] S. J. Linz and M. Lücke, Phys. Rev. A **36**, 3505 (1987).

[24] E. Knobloch and D. R. Moore, Phys. Rev. A **37**, 860 (1988).

[25] M. C. Cross and K. Kim, Phys. Rev. A **37**, 3909 (1988).

[26] W. Barten, M. Lücke, W. Hort, and M. Kamps, Phys.

Rev. Lett. **63**, 376 (1989); W. Barten, M. Lücke, and M. Kamps, *ibid.* **66**, 2621 (1991).
[27] D. Bensimon, A. Pumir, and B. I. Shraiman, J. Phys. (Paris) **50**, 3089 (1989).
[28] W. Schöpf and W. Zimmermann, Europhys. Lett. **8**, 41 (1989); Phys. Rev. A **41**, 1145 (1990).
[29] E. Knobloch and D. Moore, Phys. Rev. A **42**, 4693 (1990).
[30] M. C. Cross, Phys. Rev. Lett. **57**, 2935 (1986); Phys. Rev. A **38**, 3593 (1988).
[31] For an overview see, e.g., A. C. Newell, in *Propagation in Systems Far from Equilibrium* (Ref. [1(b)]), p. 122.
[32] See, e.g., M. Golubitsky, I. Stewart, and D. G. Schaeffer, *Singularities and Groups in Bifurcation Theory* (Springer, Berlin, 1988).
[33] G. Ahlers, P. C. Hohenberg, and M. Lücke, Phys. Rev. A **32**, 3493 (1985).
[34] A. C. Newell and J. A. Whitehead, J. Fluid Mech. **38**, 279 (1969); A. C. Newell, Lect. Appl. Math. **15**, 157 (1974).
[35] M. C. Cross, Phys. Fluids **23**, 1727 (1980).
[36] M. C. Cross, P. G. Daniels, P. C. Hohenberg, and E. D. Siggia, J. Fluid Mech. **127**, 155 (1983).
[37] E. Knobloch and M. R. E. Proctor, J. Fluid Mech. **108**, 291 (1981); P. H. Coulett and E. A. Spiegel, SIAM J. Appl. Math. **43**, 776 (1983).
[38] H. R. Brand, P. C. Hohenberg, and V. Steinberg, Phys. Rev. A **27**, 591 (1983); **30**, 2548 (1984).
[39] H. R. Brand, P. S. Lomdahl, and A. C. Newell, Physica D **23**, 345 (1986).
[40] G. Dangelmayr and E. Knobloch, Philos. Trans. R. Soc. London Ser. A **322**, 243 (1987).
[41] W. Zimmermann, D. Armbruster, L. Kramer, and W. Kuang, Europhys. Lett. **6**, 505 (1988).
[42] P. Coullet, S. Fauve, and E. Tirapegui, J. Phys. (Paris) Lett. **46**, L787 (1985).
[43] C. S. Bretherton and E. A. Spiegel, Phys. Lett. **96A**, 152 (1983).
[44] O. Thual and S. Fauve, J. Phys. (Paris) **49**, 1829 (1988); S. Fauve and O. Thual, Phys. Rev. Lett. **64**, 282 (1990).
[45] H. R. Brand and R. J. Deissler, Phys. Rev. Lett. **63**, 2801 (1989); R. J. Deissler and H. R. Brand, Phys. Lett. A **146**, 252 (1990).
[46] W. van Saarloos and P. C. Hohenberg, Phys. Rev. Lett. **64**, 749 (1990); Physica D **56**, 303 (1992).
[47] W. Schöpf and L. Kramer, Phys. Rev. Lett. **66**, 2316 (1991).
[48] See, e.g., J. Guckenheimer and P. Holmes, *Nonlinear Oscillations, Dynamical Systems and Bifurcations of Vector Fields* (Springer, New York, 1983), Chap. 7.
[49] W. Zimmermann and W. Schöpf, in Ref. [1c], p. 69.
[50] H. E. Stanley, *Introduction to Phase Transitions and Critical Phenomena* (Oxford University, Oxford, 1971).
[51] V. M. Zaĭtsev and M. I. Shliomis, Zh. Eksp. Teor. Fiz. **59**, 1583 (1970) [Sov. Phys. JETP **32**, 866 (1971)].
[52] R. Graham, Phys. Rev. A **10**, 1762 (1974).
[53] J. Swift and P. C. Hohenberg, Phys. Rev. A **15**, 319 (1977).
[54] G. Ahlers, M. C. Cross, P. C. Hohenberg, and S. Safran, J. Fluid Mech. **110**, 297 (1981); C. W. Meyer, G. Ahlers, and D. S. Cannell, Phys. Rev. Lett. **59**, 1577 (1987); Phys. Rev. A **44**, 2514 (1991).
[55] I. Rehberg, S. Rasenat, M. de la Torre Juárez, W. Schöpf, F. Hörner, G. Ahlers, and H. R. Brand, Phys. Rev. Lett. **67**, 596 (1991); I. Rehberg, F. Hörner, L. Chiran, H. Richter, and B. L. Winkler, Phys. Rev. A **44**, 7885 (1991).
[56] L. D. Landau and E. M. Lifshitz, *Fluid Mechanics* (Pergamon, London, 1959).
[57] D. A. Nield, J. Fluid Mech. **29**, 545 (1967).
[58] A. Schlüter, D. Lortz, and F. Busse, J. Fluid Mech. **23**, 129 (1965).
[59] M. A. Dominguez-Lerma, G. Ahlers, and D. S. Cannell, Phys. Fluids **27**, 856 (1984).
[60] T. Clune and E. Knobloch (unpublished); E. Knobloch (private comminication).
[61] M. R. Ardron, P. G. J. Lucas, and N. D. Stein (unpubished); P. G. J. Lucas (private communication).
[62] F. Busse, J. Fluid Mech. **30**, 625 (1967).
[63] H. Riecke, Phys. Rev. Lett. **68**, 301 (1992).
[64] L. D. Landau and E. M. Lifshitz, *Statistical Physics* (Pergamon, London, 1958).
[65] I. M. Khalatnikov, Zh. Eksp. Teor. Fiz. **3**, 809 (1957) [Sov. Phys. JETP **6**, 624 (1957)]; H. N. W. Lekkerkerker and W. G. Laidlaw, J. Phys. (Paris) **38**, 1 (1977).
[66] R. Graham (Phys. Rev. A **45**, 4198(E) (1992) (erratum to ref. [52]); and (private communication).
[67] J. Swift and P. C. Hohenberg (private communication).
[68] *Tables of Integral Transforms,* edited by A. Erdélyi (McGraw-Hill, New York, 1954), Vol. 1, Table 1.4 (15).